Research Paper

E3 ligase FBXW7 restricts M2-like tumor-associated macrophage polarization by targeting c-Myc

Lijia Zhong[1], Yuanyuan Zhang[1], Mengyao Li[1], Yinjing Song[2], Danhui Liu[3], Xin Yang[1], Dehua Yang[1], Hao Qu[4], Lihua Lai[3], Qingqing Wang[3], Zhimin Chen[1]

[1]Department of Pulmonology, The Children's Hospital, Zhejiang University School of Medicine, National Clinical Research Center for Child Health, Hangzhou 310052, China
[2]Sir Run Shaw Hospital, Zhejiang University School of Medicine, Hangzhou 310016, China
[3]Institute of Immunology, Zhejiang University School of Medicine, Hangzhou 310058, China
[4]Department of Orthopedic Surgery, The Second Affiliated Hospital of Zhejiang University School of Medicine, Hangzhou 310009, China

Correspondence to: Zhimin Chen, Qingqing Wang; **email:** zmchen@zju.edu.cn, wqq@zju.edu.cn
Keywords: FBXW7, tumor-associated macrophages, macrophage polarization, c-Myc, ubiquitination
Received: February 5, 2020 **Accepted:** September 24, 2020 **Published:** December 1, 2020

ABSTRACT

FBXW7 functions as an E3 ubiquitin ligase to mediate oncoprotein degradation via the ubiquitin-proteasome system in cancer cells, effectively inhibiting the growth and survival of tumor cells. However, little is known about the functions of FBXW7 in macrophages and the tumor immune microenvironment. In this study, we find that FBXW7 suppresses M2-like tumor-associated macrophage (TAM) polarization to limit tumor progression. We identified a significant increase in the proportion of M2-like TAMs and aggravated tumor growth in mice with myeloid FBXW7 deficiency by subcutaneous inoculation with Lewis lung carcinoma cells (LLCs). When stimulated with LLCs supernatant *in vitro*, FBXW7-knockout macrophages displayed increased M2 macrophage polarization and enhanced ability of supporting cancer cells growth. In mechanism, we confirmed that FBXW7 inhibited M2-like TAM polarization by mediating c-Myc degradation via the ubiquitin-proteasome system. These findings highlight the role of FBXW7 in M2-like TAM polarization and provide new insights into the potential targets for cancer immunotherapies.

INTRODUCTION

Macrophages are particularly abundant in the tumor immune microenvironment and their density is associated with poor prognosis of several cancers [1, 2]. Macrophages are highly plastic and are broadly classified into the pro-inflammatory subset (M1) and the immunosuppressive subset (M2) [3]. Most tumor-associated macrophages (TAMs) are polarized into the M2 subtype by specific factors expressed in the tumor microenvironment [4]. M2-like TAMs participate in cancer initiation, development and metastasis by improving the invasive properties of tumor cells, remodeling the invasive extracellular stroma, promoting angiogenesis, and benefiting tumor cells proliferation [5–10]. At the same time, M2-like TAMs mediate immunosuppression by secreting inhibitory cytokines and upregulating the expression of inhibitory receptors [11–14]. However, the detailed mechanisms of macrophage polarization and its relationship with tumorigenesis remain largely unknown. Exploring the regulators of macrophage polarization and targeting the switch that controls the direction of TAM polarization may improve the efficiency of existing cancer therapies

and lead to the development of new cancer immunotherapies [15, 16].

Ubiquitination is a common post-translational modification of intracellular proteins that plays a significant role in cell cycle, signal transduction, proliferation, apoptosis, and immune response [17–21]. Ubiquitination occurs through a cascade of enzymatic reactions involving three different classes of enzymes: ubiquitin-activating enzymes (E1), ubiquitin-conjugating enzymes (E2), and ubiquitin-ligating enzymes (E3) [22]. An abnormality in any one of these enzymes can cause many diseases, including cancer [23, 24]. The E3 ubiquitin ligase F-box and WD repeat domain-containing 7 (FBXW7) is a well-known tumor suppressor that mediates degradation of several oncoproteins including c-Myc, cyclin E, and Mcl-1, which play a critical role in regulating the cell cycle, DNA damage and repair, signal transduction, and transcription factor activity in tumor cells [24] [25]. Therefore, FBXW7 suppresses tumor cell survival and proliferation, effectively limiting cancer development. FBXW7-knockout in mouse embryonic fibroblasts decreased E-cadherin expression and induced the occurrence of epithelial-to-mesenchymal transition, which promotes tumor metastasis [26]. *FBXW7* mutations in bone marrow stromal cells (BMSCs) can increase the CCL2 expression, which promotes recruitment of immunosuppressive cells and metastasis [27]. These findings indicate that FBXW7 can affect cancer development through both tumor cells themselves and through the surrounding non-malignant cells. However, the role of FBXW7 in tumor immune microenvironment, particularly in TAM polarization, has not yet been described.

Recent studies suggest that FBXW7 can mediate CCAAT/enhancer-binding protein delta (C/EBPδ) degradation to suppress *Tlr4* expression, attenuating inflammation, and regulating the innate immune response of macrophages to pathogen [28]. Our previous study showed that FBXW7 catalyzes SHP2 degradation via the ubiquitin-proteasome system to stabilize RIG-I to promote IFN-I production in macrophages, which subsequently orchestrates innate immune response against RNA virus infection [29]. Since FBXW7 plays an integral role in macrophage function, we hypothesized that it might regulate macrophage phenotype switching in the tumor microenvironment. Here, we investigated the role of myeloid cell-specific FBXW7-knockout on tumor progression in mice and on M2-like TAMs. We found that myeloid cell-specific FBXW7-deficient ($Lysm^{+}FBXW7^{f/f}$) C57BL/6 mice showed exacerbated tumor progression and had a higher proportion of M2-like TAMs in solid tumor tissues after the subcutaneous injection of Lewis lung carcinoma cells (LLCs). FBXW7 inhibited M2 macrophage polarization and repressed the production of tumor-promoting factors with the stimulation of LLC supernatant *in vitro*. In mechanism, FBXW7 catalyzed the ubiquitination and degradation of c-Myc, which restricts M2-like macrophage polarization. Altogether, our findings clarify the previously unrecognized role of FBXW7 in regulating the function of M2-like TAMs, and provide new potential target for anti-cancer therapies.

RESULTS

FBXW7 deficiency in myeloid cells promotes tumor progression in an LLC-inoculated lung cancer model

FBXW7 mutants have been previously identified in various tumor tissues [30]. Mice with FBXW7 conditional depletion in the T cell lineages, bone marrow stromal cells could develop cancer [27]. To determine whether FBXW7 affects tumor progression by regulating the function of innate immune cells in remodeling the tumor immune microenvironment, myeloid cell-specific FBXW7-deficient ($Lysm^{+}FBXW7^{f/f}$) C57BL/6 mice were generated. After confirming the efficiency of FBXW7 knockout (Supplementary Figure 1A–1C), cells in the bone marrow and spleen from $FBXW7^{f/f}$ and $Lysm^{+}FBXW7^{f/f}$ mice were collected and analyzed by flow cytometry. We observed no significant differences between $FBXW7^{f/f}$ and $Lysm^{+}FBXW7^{f/f}$ mice in terms of the percentage of myeloid cells and lymphocytes (Supplementary Figure 1D–1I). Thus, FBXW7 knockout in myeloid cells did not affect the development of myeloid cells and lymphocytes.

Next, we injected LLCs subcutaneously into the flanks of the $FBXW7^{f/f}$ and $Lysm^{+}FBXW7^{f/f}$ mice. Tumor volume change was recorded 16 days after the injection of LLCs and was used to evaluate tumor growth. We observed increased tumor volume and accelerated tumor growth in $Lysm^{+}FBXW7^{f/f}$ mice (Figure 1A). At 16 days after injection, tumors were dissected, weighed and photographed. We found that the tumor weight was significantly increased in mice with FBXW7 knockout in myeloid cells (Figure 1B). The appearance of the tumors in two groups was evaluated (Figure 1C) and indicated that FBXW7 depletion in myeloid cells promoted tumor development. To analyze the long-term effects of FBXW7 knockout in myeloid cells on tumor prognosis, the survival rates of tumor-bearing mice were recorded. Early death was observed more commonly in $Lysm^{+}FBXW7^{f/f}$ mice than in $FBXW7^{f/f}$ mice (Figure 1D). We further analyzed the rates of tumor cell proliferation and found that Ki67 was more highly expressed in $Lysm^{+}FBXW7^{f/f}$ mice than in

FBXW7$^{f/f}$ mice (Figure 1E). Taken together, these results indicate that the Lysm^{+}FBXW7$^{f/f}$ mice show enhanced tumor progression.

FBXW7 depletion in myeloid cells promotes cancer development by facilitating M2-like TAM polarization

Tumor development is a complicated process that involves many interactions between tumor cells and the tumor microenvironment. At the onset of tumorigenesis, innate and adaptive immune cells are recruited to construct a tumorigenic immune microenvironment [31–34]. To investigate which kind of tumorigenic immune microenvironment compositions promoted tumor progression in Lysm^{+}FBXW7$^{f/f}$ mice, we compared the proportion of immune cells infiltrating the tumor tissues of FBXW7$^{f/f}$ and Lysm^{+}FBXW7$^{f/f}$ mice by flow cytometry. In innate immune cells, the percentage of Ly6C^{+}CD11b^{+} myeloid-derived suppressor cells (MDSCs), Ly6G^{+}CD11b^{+} MDSCs, and MHCII^{+}CD11c^{+} dendritic cells were comparable between the two groups (Figure 2A, 2B). This suggested that these cells were not the cause of the difference in tumor progression observed between FBXW7$^{f/f}$ and Lysm^{+}FBXW7$^{f/f}$ mice.

Macrophages are the most abundant immune cells in the tumor stroma. Hypoxia, lactate, and other factors in tumor microenvironment promote M2-like TAMs polarization [4]. In turn, M2-like TAMs support tumor growth and metastasis through intercellular communication and by producing mediators to shape the tumor microenvironment [16, 35]. According to our data, although the percentage of macrophages (F4/80^{+}CD11b^{+}) infiltrating the tumor tissues was no different between FBXW7$^{f/f}$ and Lysm^{+}FBXW7$^{f/f}$ mice, a higher percentage of CD206^{+} subset in macrophages was observed in the FBXW7-knockout group (Figure 2C, 2D). These results indicate that conditional FBXW7 knockout may switch the TAM phenotype and facilitate polarization to the M2 subset, thus benefiting tumor growth.

Lymphocytes also serve as important and direct anti-tumor effector cells [36, 37]. We detected CD3^{+}, CD4^{+}, and CD8^{+} lymphocytes from single-cell suspensions of tumor tissues by flow cytometry. There were no significant differences in the proportion of CD3^{+} T cells, CD4^{+} T cells, and CD8^{+} T cells between FBXW7$^{f/f}$ and Lysm^{+}FBXW7$^{f/f}$ mice (Figure 2E, 2F), suggesting that FBXW7 knockout did not influence the proportion of the lymphocytes in tumor tissues.

The neutrophil is one of granulocyte expressing a high level of Lyz2 and contributes significantly to cancer development [33, 38]. To examine whether neutrophils are related to the aggravated tumor progression observed in Lysm^{+}FBXW7$^{f/f}$ mice, we depleted neutrophils using an anti-Ly6G Ab (Supplementary Figure 2A, 2B). Anti-Ly6G Ab reduced neutrophil recruitment in tumor tissues but did not abolish the difference in tumor progression between FBXW7$^{f/f}$ and Lysm^{+}FBXW7$^{f/f}$ mice (Supplementary Figure 2C–2G). Interestingly, Lysm^{+}FBXW7$^{f/f}$ mice showed enhanced tumor progression compared to FBXW7$^{f/f}$ mice, with a higher percentage of CD206^{+} macrophages in the tumor tissue, regardless of neutrophil depletion (Supplementary Figure 2H, 2I). These findings indicated that the function of conditional FBXW7 knockout in tumors might be dependent on M2-like TAMs rather than on neutrophils.

To further determine whether the ablation of FBXW7 was responsible for the increase in M2-like TAMs in the tumor microenvironment, we subsequently detected mRNA expression of the immunosuppressive factors Arginase 1 (*Arg1*), resistin like alpha (*Fizz1*), and chitinase-like 3 (*Ym1)* as markers of M2-polarized macrophages in tumor tissues. Higher levels of *Arg1*, *Fizz1*, and *Ym1* were found in the Lysm^{+}FBXW7$^{f/f}$ mice compared to the FBXW7$^{f/f}$ mice (Figure 2G). Next, we analyzed changes in the expression of vascular endothelial growth factor α (*VEGFα*) and matrix metalloproteinase 9 (*MMP9*), which are produced by M2-like TAMs to support tumor growth by inducing neovascularization and modifying the extracellular matrix (ECM) [39, 40]. Both factors showed higher levels in the Lysm^{+}FBXW7$^{f/f}$ mice compared to the FBXW7$^{f/f}$ mice (Figure 2G). Collectively, these data demonstrate that FBXW7 knockout promotes cancer development by facilitating M2-like TAM polarization to modify the microenvironment.

FBXW7 knockout facilitates M2 macrophage polarization *in vitro*

To further determine the role of FBXW7 in the polarization of M2-like TAMs, we stimulated macrophages with LLC supernatant to mimic the lung cancer condition and detected the expression of FBXW7 in M2 macrophages. The gene and protein expression of Arg1 and Ym1, markers of the M2 phenotype, gradually increased in peritoneal macrophages over time. Simultaneously, FBXW7 expression decreased at both the mRNA and protein levels in early time (Figure 3A, 3B). Similar results were observed in bone marrow derived macrophages (BMDMs) (Figure 3C, 3D). Therefore, we assumed that the expression of FBXW7 played a role in the regulation of M2 macrophage polarization.

To further confirm this hypothesis, we treated peritoneal macrophages and BMDMs from FBXW7$^{f/f}$ and

Lysm^{+}FBXW7$^{f/f}$ mice with LLC supernatant. We found that higher mRNA levels of *Arg1*, *Fizz1*, and *Ym1* were expressed in FBXW7-knockout peritoneal macrophages compared to the wild-type peritoneal macrophages (Figure 4A). At the protein level, Arg1 and Ym1 levels were increased to a greater extent due to FBXW7 knockout, as confirmed by immunoblotting (Figure 4B). Similar results were observed in BMDMs under the same conditions (Figure 4C, 4D). Subsequently, we performed F4/80 and CD206 staining to examine the proportion of CD206^{+} M2 macrophages in stimulated peritoneal macrophages and BMDMs by flow cytometry. The percentage of CD206^{+} M2 macrophages was higher in FBXW7-knockout macrophages than in

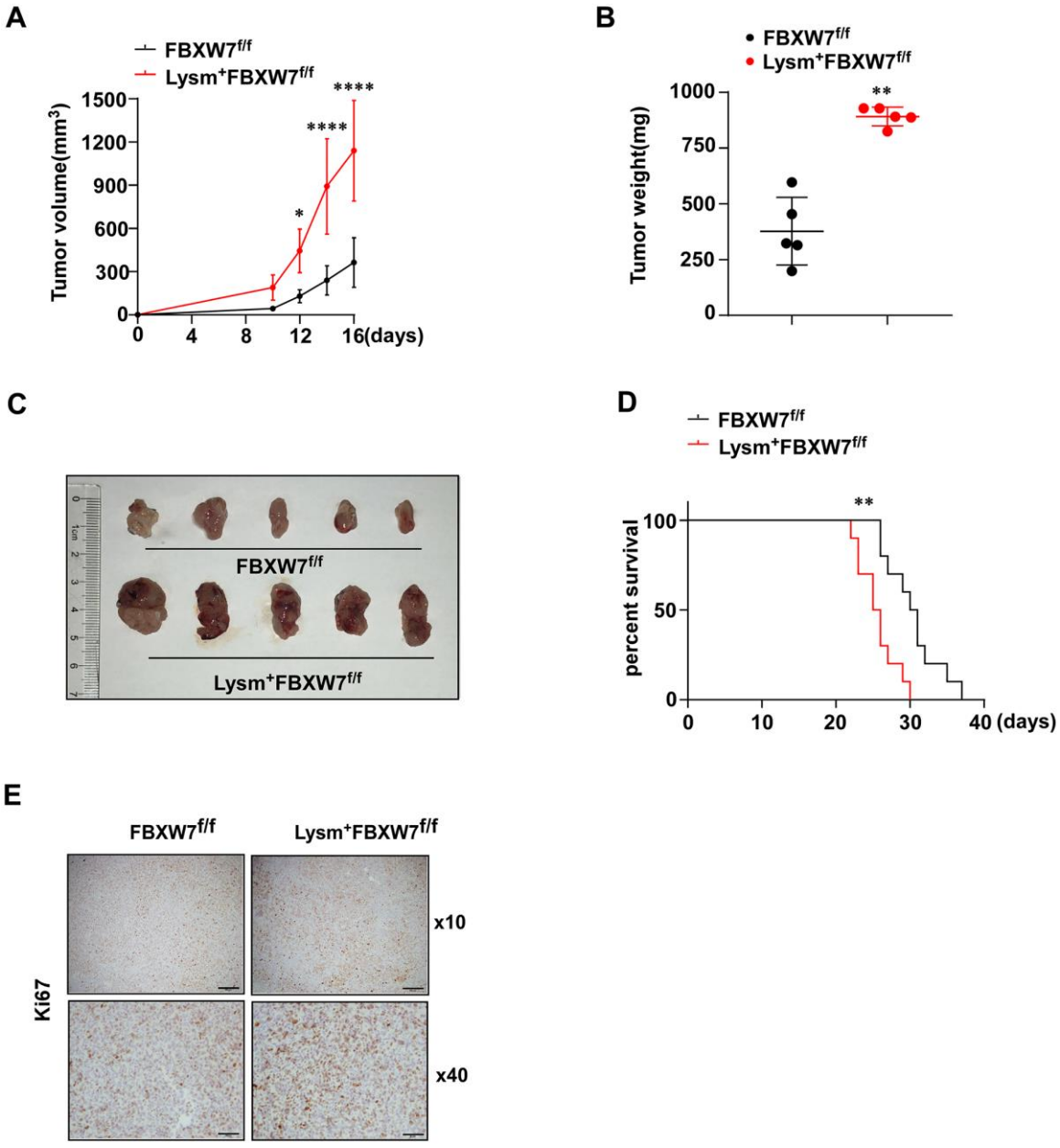

Figure 1. Lysm^{+}FBXW7$^{f/f}$ mice show aggravated tumor progression in an LLC-inoculated model. (**A**) LLCs were subcutaneously injected into the mice. The volume of tumors from FBXW7$^{f/f}$ and Lysm^{+}FBXW7$^{f/f}$ mice were measured and recorded in 16 days (n = 5 per group). (**B**) The weight of tumors at 16 days from both groups (n = 5 per group). (**C**) The appearance of tumors dissected 16 days after inoculation in FBXW7$^{f/f}$ and Lysm^{+}FBXW7$^{f/f}$ mice. (**D**) The survival curve of tumor-bearing FBXW7$^{f/f}$ and Lysm^{+}FBXW7$^{f/f}$ mice (n = 10 per group). (**E**) Representative images of tumors from two groups immunohistochemically stained with an antibody against Ki67. Scale bars: 10× was 200 μm, 40× was 50 μm. Data are expressed as the mean ± SD and are representative of three independent experiments. **P* < 0.05; ***P* < 0.01; *****P* < 0.0001 (two-way ANOVA (**A**), Student's t test (**B**) and log rank test (**D**)).

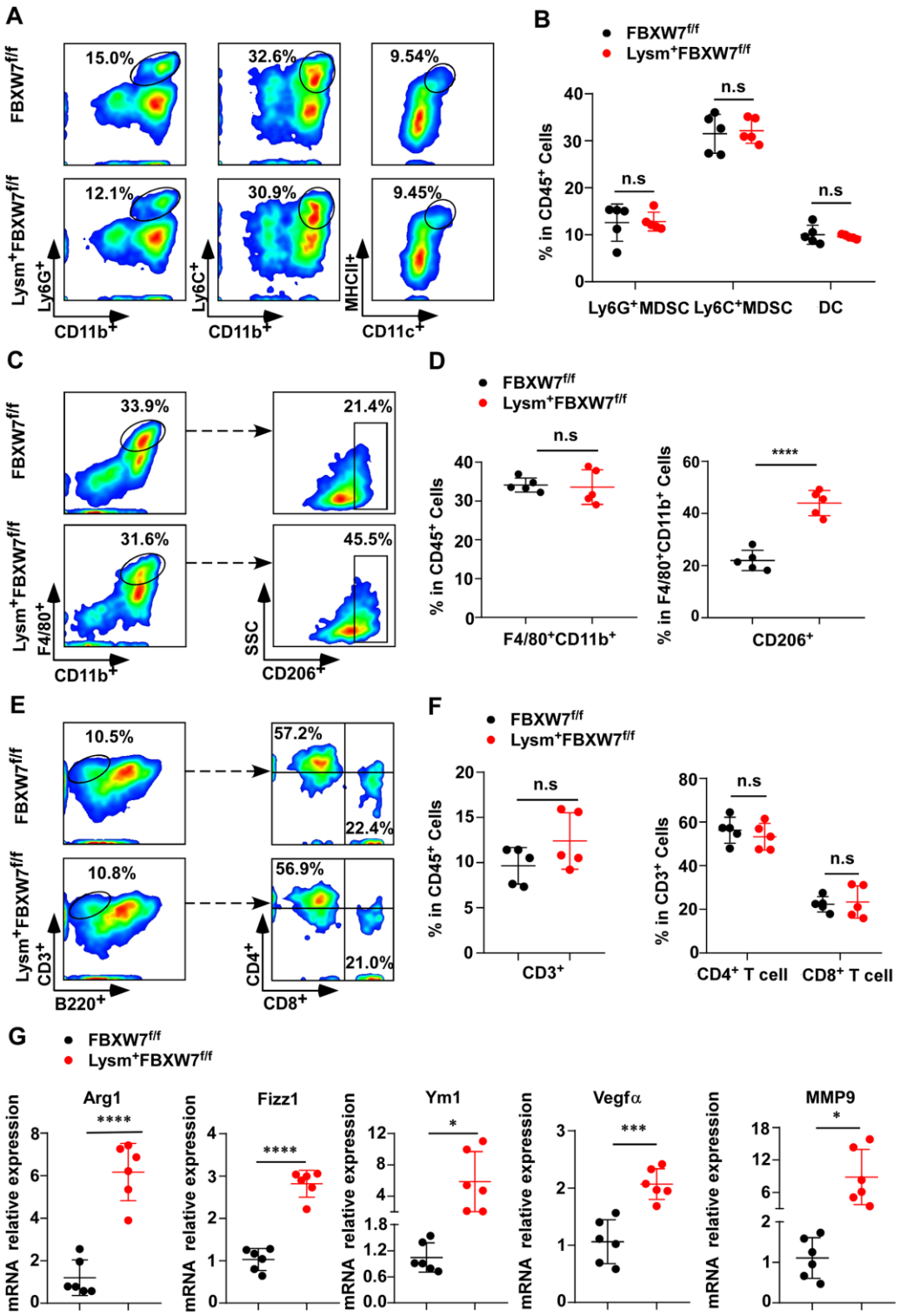

Figure 2. FBXW7 knockout in myeloid cells remodels the tumor immune microenvironment by promoting M2-like TAM polarization. (**A**) Tumors were digested to obtain single-cell suspensions. $Ly6G^+CD11b^+$ myeloid-derived suppressor cells (MDSCs), $Ly6C^+CD11b^+$ MDSCs, and $MHCII^+CD11c^+$ dendritic cells in the tumors were analyzed by flow cytometry. (**B**) Statistical analysis of the results in (**A**) (n = 5 per group). (**C**, **D**) Flow cytometry analysis (**C**) and statistical analysis (**D**) of $F4/80^+CD11b^+$ macrophages and $CD206^+$ macrophages in tumors (n = 5 per group). (**E**, **F**) Flow cytometry analysis (**E**) and statistical analysis (**F**) of $CD3^+$ T cells infiltrating the tumor, $CD4^+$ and $CD8^+$ T cells in $CD3^+$ T cells (n = 5 per group). (**G**) Relative mRNA expression of *Arg1, Fizz1, Ym1, VEGFα,* and *MMP9* in tumors was measured by qRT-PCR (n = 6 per group). Data are shown as the mean ± SD and are representative of three independent experiments. *P < 0.05; ***P < 0.001; ****P < 0.0001; n.s, no significance (Student's t test (**B**, **D**, **F**, **G**)).

wild-type macrophages (Figure 4E–4H). Altogether, our results revealed that FBXW7 knockout facilitated M2 macrophage polarization after incubation with LLC supernatant, consistent with the observed function of FBXW7 in our LLC-inoculated mouse model.

As reported in previous studies, macrophage polarization is triggered by multiple stimuli [3, 41]. In addition to LLC supernatant, we used IL-4, a classical M2 macrophage-inducing factor, to polarize macrophages derived from $FBXW7^{f/f}$ and $Lysm^{+}FBXW7^{f/f}$ mice and compared M2 markers expression. The gene and protein expression of Arg1, Fizz1, and Ym1 were substantially higher in FBXW7-knockout M2 macrophages under IL-4 stimulation (Supplementary Figure 3A–3D). Flow cytometry analysis also demonstrated that FBXW7 knockout promoted IL-4-induced M2 macrophage polarization, with a significantly higher proportion of $CD206^{+}$ macrophages (Supplementary Figure 3E–3H). Taken together, FBXW7 knockout enhances M2-associated gene expression at both the mRNA and protein levels following multiple stimuli.

We also analyzed the regulation of FBXW7 in the human monocyte cell line, THP-1. We silenced FBXW7 with small interfering RNA (siRNA) in THP-1 cells and found significantly increased expression of the M2 macrophage markers; Arg1, CD163, transforming growth factor β (TGFβ), and IL10 in FBXW7-silenced THP1 cells after A549 supernatant treatment compared to the unsilenced THP-1 cells (Supplementary Figure 4A–4E).

These data demonstrate that FBXW7 plays an integral role in M2 macrophage polarization.

FBXW7 knockout promotes expression of pro-tumoral factors in macrophages

M2-like TAMs contribute to tumor progression by expressing VEGFα to benefit angiogenic process

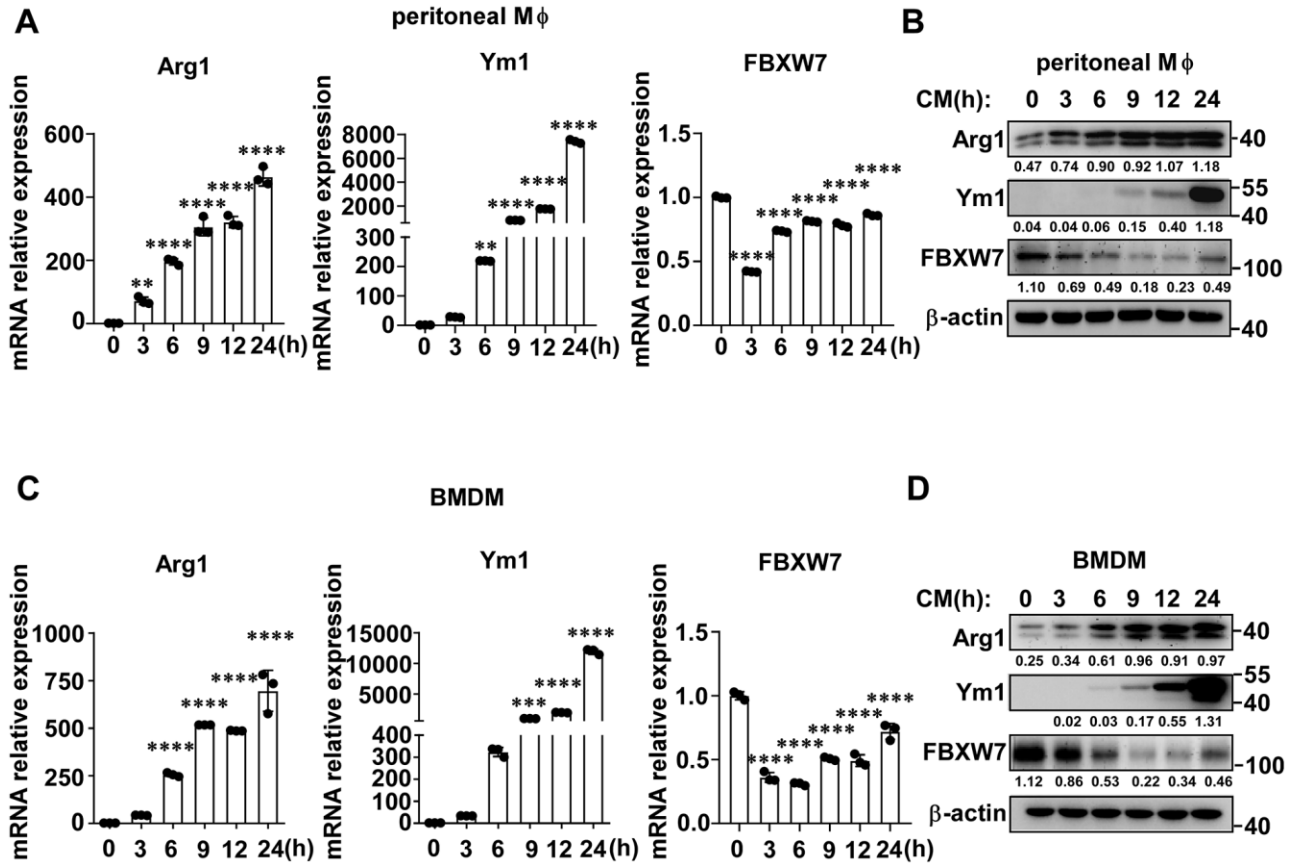

Figure 3. FBXW7 expression decreases in M2-like TAMs. (**A**, **B**) Peritoneal macrophages were stimulated with conditioned medium containing LLC supernatant for the indicated time periods. The mRNA (**A**) and protein (**B**) expression levels of Arg1, Ym1, and FBXW7 were measured by qRT-PCR and immunoblotting, respectively. (**C**, **D**) BMDMs were incubated in conditioned medium, and the mRNA (**C**) and protein (**D**) expression levels of Arg1, Ym1, and FBXW7 were measured by qRT-PCR and immunoblotting. Data are shown as the mean ± SD and are representative of three independent experiments. n=3. $^{**}P < 0.01$; $^{***}P < 0.001$; $^{****}P < 0.0001$ (one-way ANOVA (**A**, **C**)).

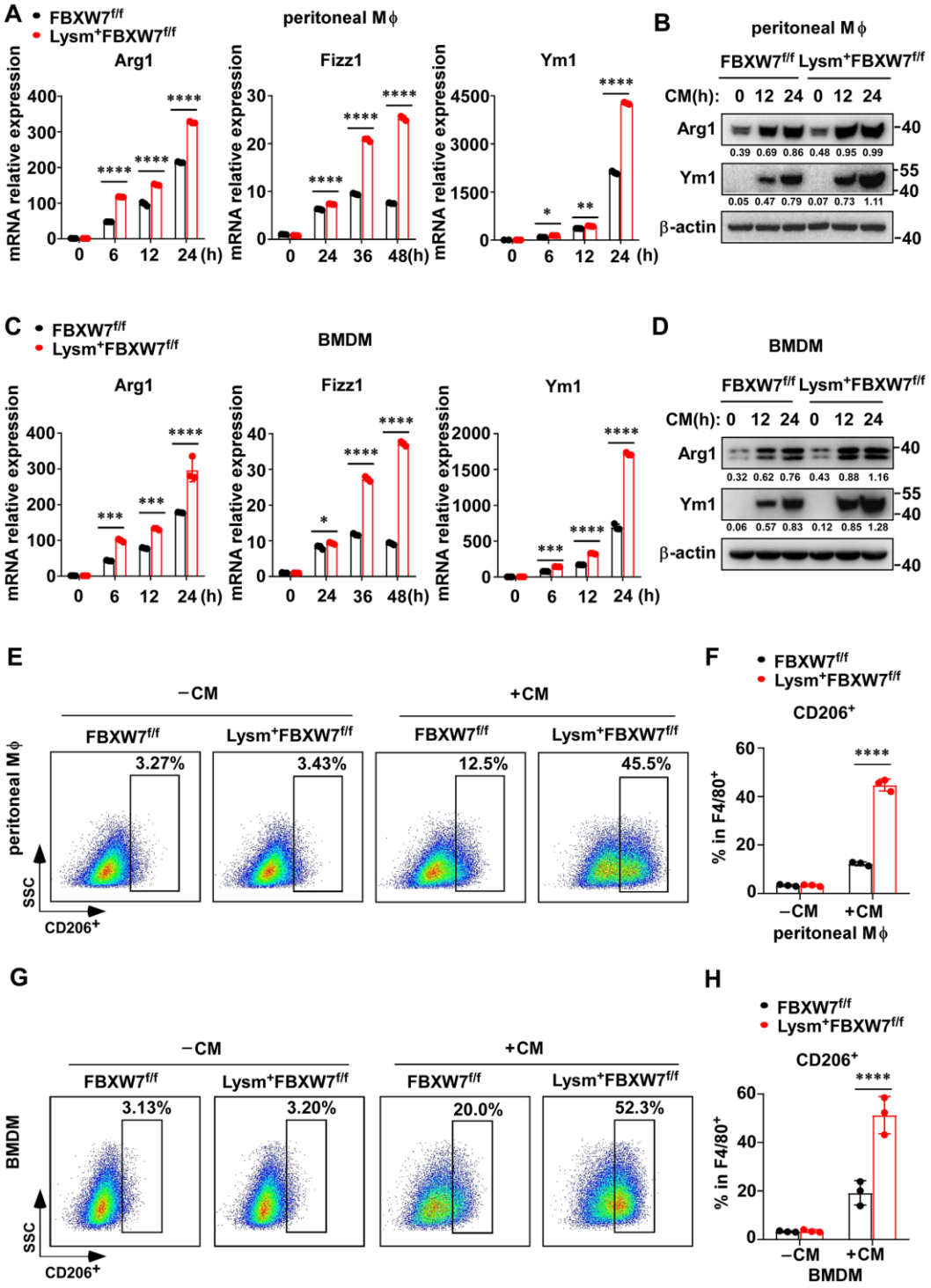

Figure 4. FBXW7 knockout facilitates M2 macrophage polarization in a tumor microenvironment-mimicking condition. (**A**) Peritoneal macrophages extracted from FBXW7$^{f/f}$ and Lysm^{+}FBXW7$^{f/f}$ mice were treated with conditioned medium containing LLC supernatant. The mRNA expression of *Arg1*, *Fizz1*, and *Ym1* were analyzed by qRT-PCR. (**B**) The protein levels of Arg1 and Ym1 in wild-type and FBXW7-knockout peritoneal macrophages were detected by immunoblotting after conditioned medium stimulation. (**C**, **D**) The mRNA (**C**) and protein (**D**) expression of Arg1, Fizz1, and Ym1 were analyzed by qRT-PCR and western blotting, respectively, in BMDMs incubated with conditioned medium. (**E**, **F**) Flow cytometry analysis (**E**) and statistical analysis (**F**) of the percentage of M2 macrophages (CD206^{+}) in wild-type and FBXW7-knockout peritoneal macrophages stimulated with conditioned medium (n = 3 per group). (**G**, **H**) Flow cytometry analysis (**G**) and statistical analysis (**H**) of the percentage of M2 macrophages (CD206^{+}) in wild-type and FBXW7-knockout BMDMs stimulated with conditioned medium (n = 3 per group). Data are shown as the mean ± SD and are representative of three independent experiments. **P* < 0.05; ***P* < 0.01; ****P* < 0.001; *****P* < 0.0001 (two-way ANOVA (**A**, **C**, **F**, **H**)).

[42, 43], producing MMP9 to promote tumor invasion [40], secreting IL-10 and TGFβ to maintain an immunosuppressive microenvironment [44]. Therefore, we further investigated whether FBXW7 affected the cancer-promoting function of M2 macrophages. We stimulated peritoneal macrophages and BMDMs from FBXW7$^{f/f}$ and Lysm^{+}FBXW7$^{f/f}$ mice with LLC supernatant, and examined the expression of these representative pro-tumoral factors. We found that the mRNA levels of *MMP9*, *TGFβ*, *IL-10*, and *VEGFα* increased in both wild-type and FBXW7-knockout macrophages following stimulation. Furthermore, significantly higher mRNA expression of *MMP9*, *TGFβ*, *IL-10*, and *VEGFα* was observed in FBXW7-knockout macrophages, compared to the wild-type macrophages (Figure 5A, Supplementary Figure 5A). The protein levels of MMP9, TGFβ, IL-10, and VEGFα, detected by immunoblotting or ELISA, raised to a greater extent in FBXW7-knockout macrophages than in wild-type macrophages following stimulation (Figure 5B, 5C and Supplementary Figure 5B, 5C). Next, we cultured wild-type and FBXW7-knockout macrophages with IL-4 to induce M2-phenotype polarization and collected their supernatants. LLCs were separately cultured with serum-free RPMI-1640 medium, the supernatant of wild-type or FBXW7-knockout M2 macrophages. We examined the proliferation of LLCs at the indicated time points via MTT assay, and found that the M2 macrophage supernatant clearly facilitated cancer cells proliferation than the medium group. This effect was enhanced with FBXW7 knockout M2 macrophage supernatant than with the wild-type M2 macrophage supernatant (Figure 5D). Therefore, it suggests that FBXW7-knockout promotes pro-tumoral factors production in M2 macrophages and aggravates tumor progression upon M2 polarization.

To further determine whether the effect of FBXW7 knockout on M2 macrophage polarization was indeed responsible for tumor progression, we subcutaneously injected wild-type C57BL/6 mice with a mixture of LLCs and FBXW7$^{f/f}$ or Lysm^{+}FBXW7$^{f/f}$ M2-polarized macrophages at a 1:1 ratio (Figure 5E). We recorded the tumor volume at different time points and the tumor weight at 19 days. Co-injection with LLCs and FBXW7-knockout M2 macrophages resulted in larger tumor volume (Figure 5F) and heavier tumors (Figure 5G), which was also confirmed visually (Figure 5H).

Altogether, these results illustrate that FBXW7 knockout promotes M2 macrophage polarization and leads to the production of cancer-promoting factors by M2 macrophages.

The inhibition of FBXW7 in M2 macrophage polarization is dependent on c-Myc

Multiple molecules have been identified as crucial mediators in macrophage polarization, including STAT6, MAPK, AKT, and c-Myc [45–50]. We compared the differences in the expression of these activated downstream signaling molecules in M2 macrophages between wild-type and FBXW7-knockout macrophages after LLC supernatant stimulation. We found that the protein levels of ERK, STAT6, JNK, AKT, and c-Myc were all increased in both groups to some degree after incubation in conditioned medium, and an increase in the phosphorylation of these proteins was also observed. However, their expression and phosphorylation levels were comparable between the two groups, except for c-Myc. We found that c-Myc phosphorylation greatly increased in FBXW7-knockout macrophages stimulated with LLC supernatant (Figure 6A, 6B). Furthermore, the total protein expression of c-Myc was also higher in the FBXW7-knockout group compared to that in the wild-type group (Figure 6A, 6B).

c-Myc is a transcription factor that contributes to cellular growth, cell survival, and cell transformation [51–53], as well as a well-known oncogene. Recently, c-Myc was identified as essential for the polarization of M2-like TAMs in human colon cancer [50]. To further determine the function of c-Myc in M2-like TAMs, and whether c-Myc was responsible for the regulation of FBXW7 in M2 macrophage polarization, we transfected FBXW7$^{f/f}$ or Lysm^{+}FBXW7$^{f/f}$ macrophages with siRNA targeting c-Myc, and later stimulated the cells with LLC supernatant. We confirmed the interference efficiency of c-Myc siRNA (Figure 6C) and analyzed the protein and mRNA expression of M2-associated genes. The protein expression of Arg1 and Ym1 significantly decreased due to c-Myc interference in both groups (Figure 6D), consistent with the known positive role of c-Myc in M2 macrophage polarization [50]. Furthermore, c-Myc knockdown using siRNA abolished the discrepancy between the wild-type and FBXW7 knockout macrophages induced by LLC supernatant at the protein levels of Arg1 and Ym1 (Figure 6D). A similar result was observed in terms of the mRNA levels of *Arg1*, *Fizz1*, and *Ym1* (Figure 6E). Next, we compared the proportion of CD206^{+} macrophages in the wild-type and FBXW7-knockout macrophages after c-Myc knockdown and stimulation with conditioned medium. The difference in the proportion of CD206^{+} macrophages caused by FBXW7 knockout was discarded after c-Myc interference (Figure 6F, 6G).

In addition, we detected pro-tumor factors expression of wild-type and FBXW7-knockout macrophages after c-Myc interference. The mRNA and protein expression of

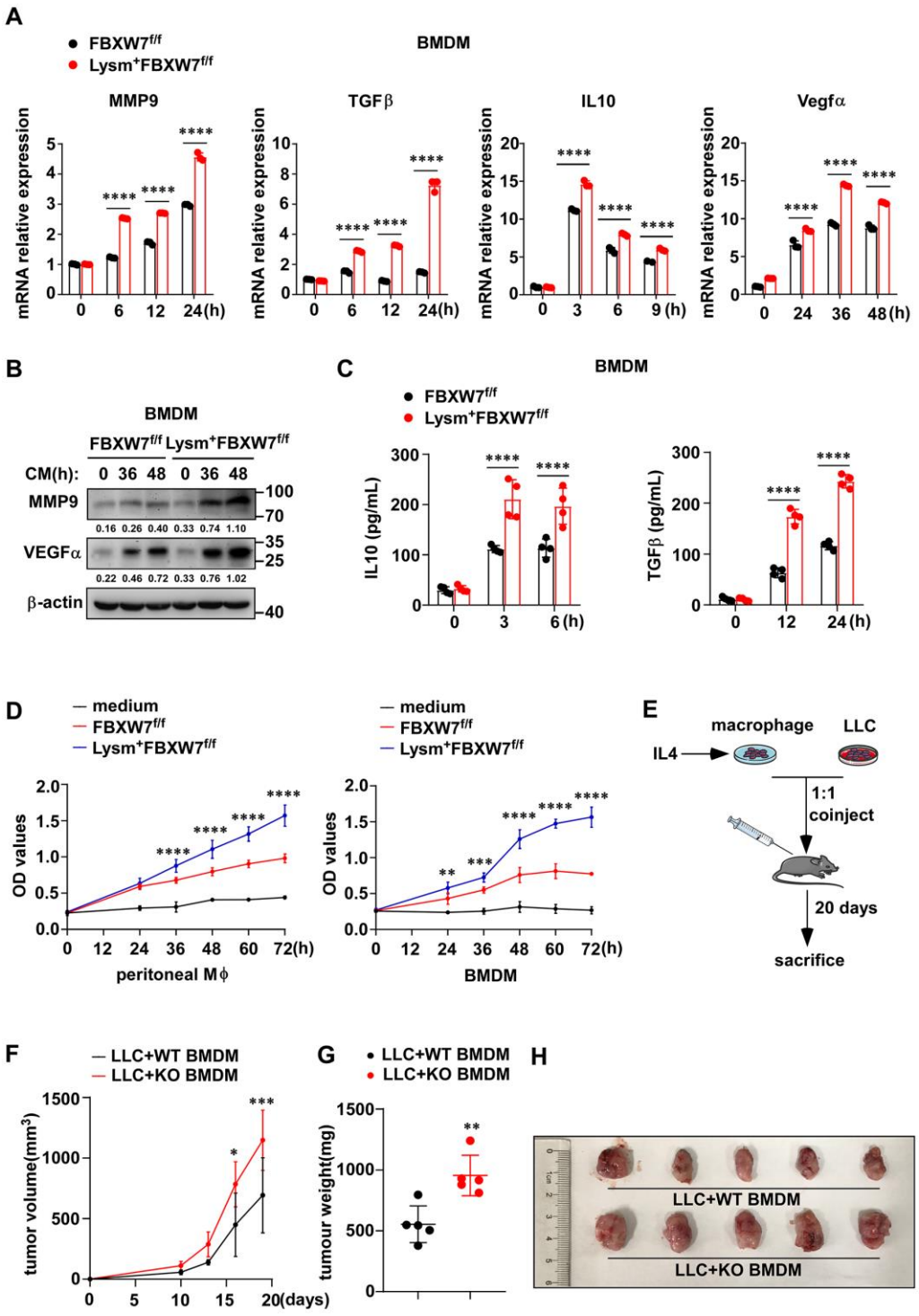

Figure 5. FBXW7 knockout promotes macrophage expressing pro-tumoral factors. (**A**) BMDMs from FBXW7$^{f/f}$ and Lysm^{+}FBXW7$^{f/f}$ mice were stimulated with conditioned medium, and the mRNA expression of *MMP9*, *IL-10, TGFβ*, and *VEGFα* was examined by qRT-PCR. (**B**) The protein expression of MMP9 and VEGFα in BMDMs incubated with conditioned medium were detected by immunoblotting. (**C**) The protein levels of IL10 and TGFβ in the supernatant of BMDMs which co-cultured with LLCs for indicated time were measured by ELISA kit. (**D**) LLCs were cultured in serum-free RPMI-1640, supernatant from IL-4-induced wild-type or FBXW7-knockout macrophages. The proliferation of LLCs in three groups was measured by MTT assay. (**E**) Schematic representation of the co-injection experimental approach. IL4-induced BMDMs derived from FBXW7$^{f/f}$ and Lysm^{+}FBXW7$^{f/f}$ mice were mixed with LLCs at a ratio of 1:1 and injected subcutaneously into healthy wild-type C57BL/6 mice. (**F**, **G**) The volume (**F**) and weight (**G**) of tumors in co-injection mice. (**H**) The appearance of tumors in two groups inoculated with a mixture of M2 macrophages and LLCs. Data are shown as the mean ± SD and are representative of three independent experiments. **P* < 0.05; ***P* < 0.01; ****P* < 0.001; *****P* < 0.0001 (two-way ANOVA (**A**, **C**, **D**, **F**) and Student's t test (**G**)).

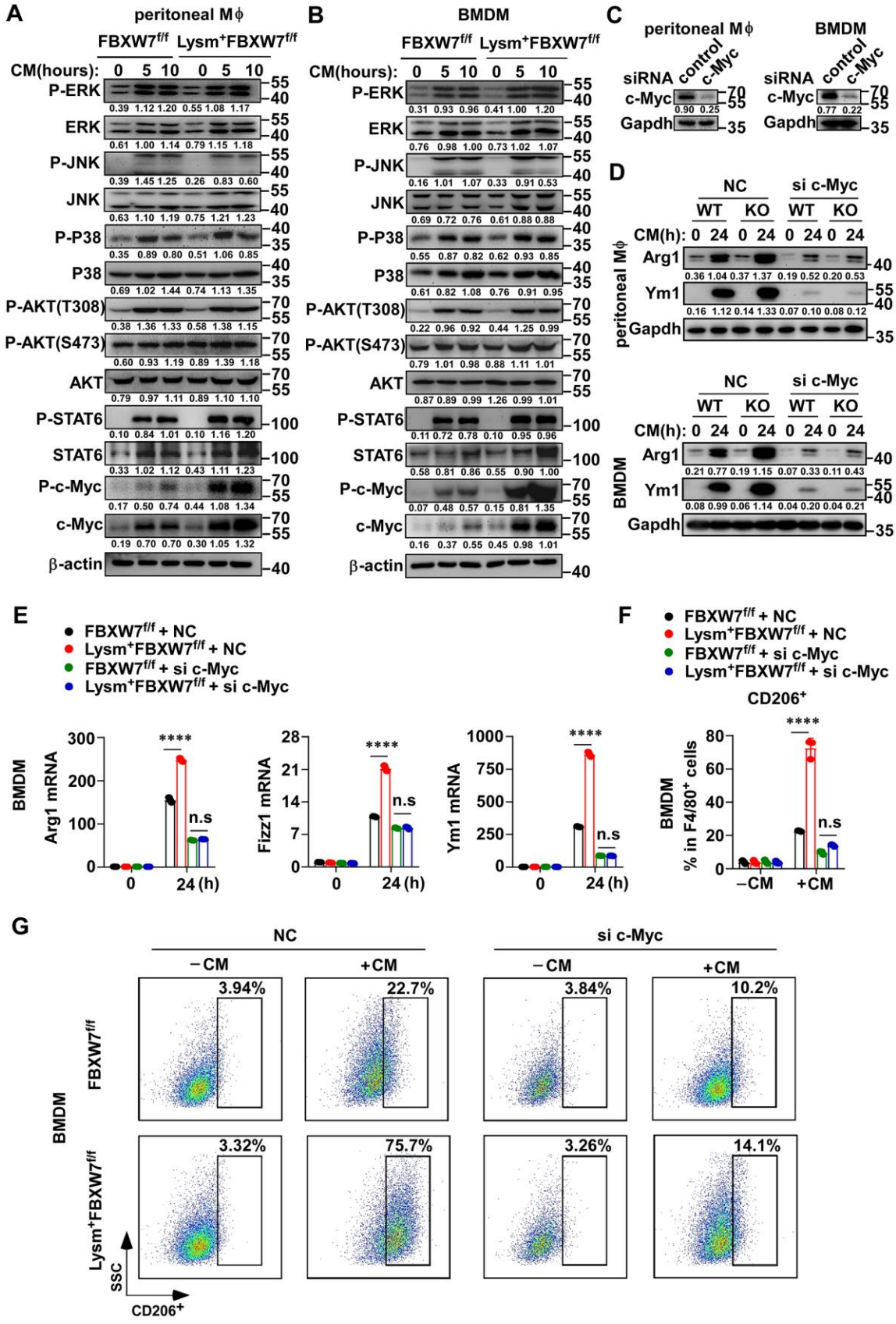

Figure 6. The role of FBXW7 in regulating M2 macrophage polarization is dependent on c-Myc. (**A**, **B**) Peritoneal macrophages (**A**) and BMDMs (**B**) derived from FBXW7$^{f/f}$ and Lysm^{+}FBXW7$^{f/f}$ mice were stimulated with conditioned medium for the indicated time periods.

The phosphorylated or total proteins related to M2 macrophage polarization were analyzed by immunoblotting. (**C**) Immunoblotting was used to analyze the interference efficiency of c-Myc siRNA in primary macrophages following stimulation with conditioned medium for 12 hours. (**D**, **E**) Immunoblotting (**D**) and qRT-PCR analysis (**E**) of Arg1 and Ym1 expression in primary macrophages from $FBXW7^{f/f}$ and $Lysm^{+}FBXW7^{f/f}$ mice transfected with or without c-Myc siRNA and stimulated with conditioned medium. (**F**, **G**) Statistical analysis (**F**) and flow cytometry analysis (**G**) of the percentage of M2 macrophages ($CD206^{+}$) in wild-type and FBXW7-knockout macrophages transfected with or without c-Myc siRNA and stimulated with conditioned medium. Data are shown as the mean ± SD and are representative of three independent experiments. ****$P < 0.0001$; n.s, no significance (two-way ANOVA (**E**, **F**)).

MMP9, TGFβ, IL-10, and VEGFα were inhibited with c-Myc knockdown. Likewise, the discrepancy of these factors expression between wild-type and FBXW7-knockout macrophages reduced to some degree (Supplementary Figure 6A–6C). Subsequently, we examined the relationship between c-Myc and FBXW7 in M2 macrophages on LLC proliferation. We collected the supernatant of wild-type and FBXW7-knockout macrophages that transfected with or without c-Myc siRNA to culture LLCs and detected the LLC proliferation rates via MTT assay. The result showed that c-Myc knockdown abolished the difference in the LLC proliferation rates between wild-type and FBXW7-knockout macrophages (Supplementary Figure 6D).

Collectively, these data indicated that the effect of FBXW7 knockout on M2-like TAM polarization and on the cancer-promoting function of M2 macrophages was dependent on c-Myc.

FBXW7 mediates the ubiquitination and degradation of c-Myc in M2 macrophages

Previous studies have shown that the E3 ubiquitin ligase FBXW7 mediates the ubiquitination and proteasome-dependent degradation of c-Myc [54–56]. Therefore, we investigated whether FBXW7 could influence the stability of c-Myc to regulate M2 macrophage polarization. We analyzed c-Myc expression in M2 macrophages incubated with the LLC supernatant, and found that the levels of c-Myc in the wild-type group increased at first and gradually declined later. However, in FBXW7-knockout M2 macrophages, c-Myc increased and did not decrease over time, and the expression of c-Myc in the FBXW7-knockout group was higher than in the wild-type group at all time points (Figure 7A). In contrast to the c-Myc expression trend, the FBXW7 expression in wild-type macrophages stimulated with LLC supernatant decreased initially and gradually increased at late (Figure 3C, 3D and Figure 7A). This suggested that FBXW7 played a role in c-Myc accumulation in M2 macrophages. We further analyzed the mRNA levels of *c-Myc* in wild-type and FBXW7-knockout M2 macrophages. The mRNA expression of *c-Myc* similarly increased in both groups (Figure 7B), suggesting that FBXW7 depletion exerted an effect on c-Myc at the post-translational level, rather than during transcription.

Next, we treated macrophages with cycloheximide (CHX) to block protein synthesis to analyze the half-life of c-Myc. The half-life of c-Myc was markedly extended in FBXW7-knockout macrophages compared to that in wild-type macrophages (Figure 7C, 7D). Subsequently, we used MG132 to inhibit proteasome-dependent degradation, and found that the difference in protein expression of c-Myc caused by FBXW7 knockout was rescued (Figure 7E). These results indicated that FBXW7 knockout attenuated c-Myc degradation and promoted c-Myc accumulation in M2 macrophages.

The E3 ligase FBXW7 catalyzes the ubiquitination of targeted substrates by recognizing a typical sequence motif called the conserved Cdc4 phosphodegron (CPD) motif. The CPD motif contains phosphorylated threonine or serine residues at positions “0” and “+4” [25]. To further investigate the interaction between FBXW7 and c-Myc, we analyzed the amino acid sequence of c-Myc among different species and found that c-Myc contained the CPD of FBXW7 (Figure 7F). We analyzed the endogenous interactions between FBXW7 and c-Myc by co-immunoprecipitation and found that FBXW7 interacted with c-Myc in M2 macrophages. A similar result was observed in reciprocal co-immunoprecipitation experiments (Figure 7G).

FBXW7 catalyzes the K48-linked polyubiquitination of c-Myc and mediates its degradation via the ubiquitin-proteasome system [54, 55]. Therefore, we examined whether FBXW7 would catalyze c-Myc K48-linked polyubiquitination in M2 macrophages. The FBXW7 knockout resulted in an inhibition of c-Myc K48-linked ubiquitination in M2 macrophages compared to in wild-type (Figure 7H).

In conclusion, these data demonstrated that FBXW7 interacted with c-Myc and catalyzed c-Myc K48-linked polyubiquitination to decrease its stability in M2 macrophages.

DISCUSSION

In this study, we demonstrate that myeloid cell-specific FBXW7 deficiency can promote tumor progression and increase the proportion of M2-like

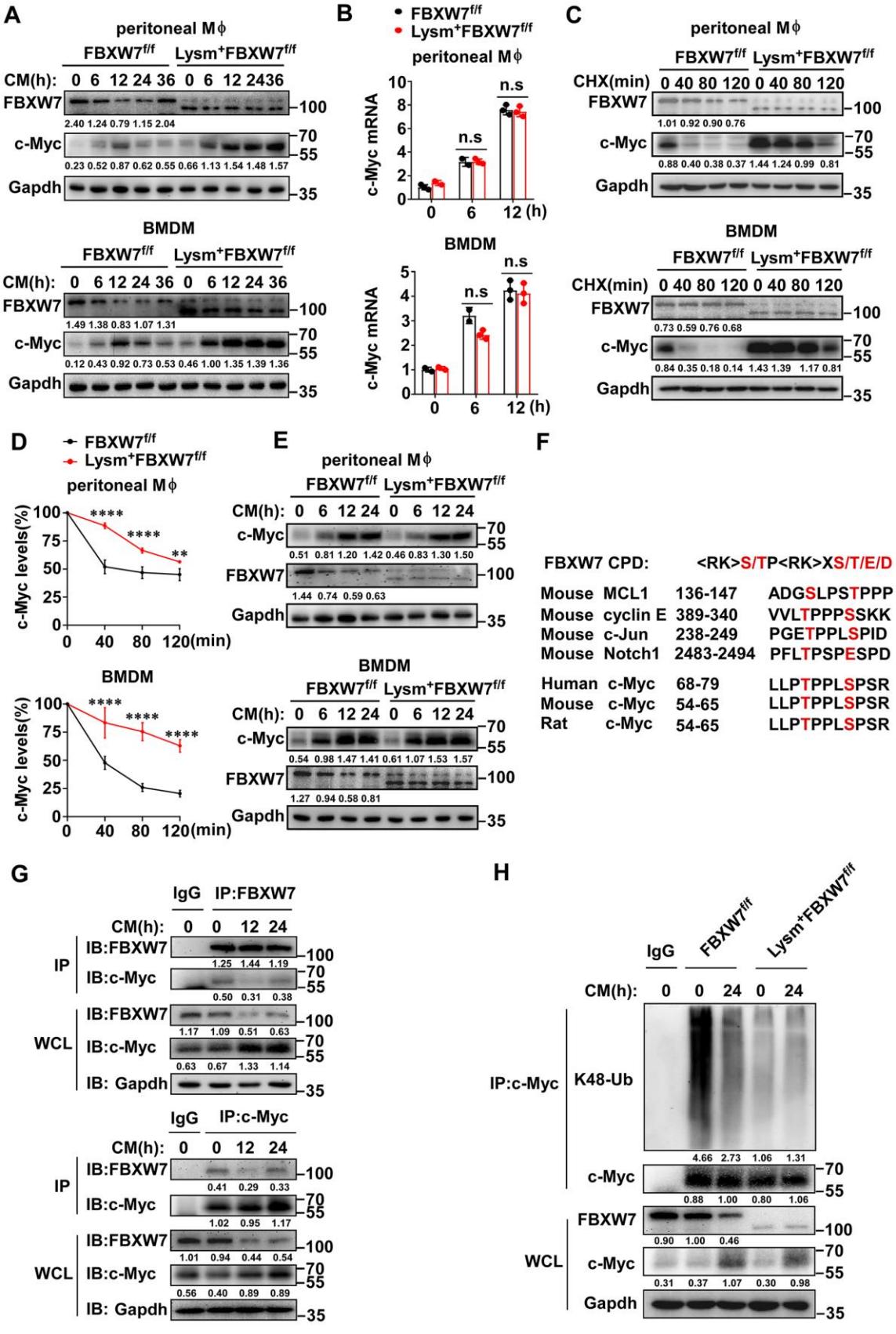

Figure 7. FBXW7 mediates degradation and ubiquitination of c-Myc in M2-like TAMs. (**A**) The protein expression of c-Myc and FBXW7 in wild-type and FBXW7-knockout primary macrophages stimulated with conditioned medium were measured by immunoblotting.

(**B**) qRT-PCR analysis of *c-Myc* mRNA expression in wild-type and FBXW7-knockout primary macrophages after conditioned medium treatment. (**C**) Immunoblot analysis of c-Myc and FBXW7 in wild-type and FBXW7-knockout primary macrophages treated with CHX (20 μg/mL) for the indicated time period after conditioned medium pre-treatment. (**D**) The quantification of relative c-Myc levels in (**C**). (**E**) The protein expression of c-Myc and FBXW7 in wild-type and FBXW7-knockout primary macrophages after treatment with MG132 (10 μM) and conditioned medium. (**F**) The phosphodegron sequence alignment of c-Myc recognized by FBXW7 with MCL1, cyclin E, Notch1, and c-Jun. The FBXW7 phosphodegron sequence present in c-Myc is conserved across different species. Conserved residues within the degron sequences are shown in red. (**G**) Immunoblot analysis of BMDMs stimulated with conditioned medium for the indicated time periods and treated with MG132, followed by immunoprecipitation with specific antibody-conjugated agarose or immunoglobulin G (IgG)-conjugated agarose. (**H**) Immunoblot analysis of the K48 ubiquitination of c-Myc in wild-type and FBXW7-knockout BMDMs stimulated with conditioned medium. Data are shown as the mean ± SD and are representative of three independent experiments. **P* < 0.05; ***P* < 0.01; ****P* < 0.001; *****P* < 0.0001; n.s, no significance (two-way ANOVA (**B**, **D**)).

TAMs in tumor tissues after subcutaneous inoculation with LLCs. We find that FBXW7 plays a critical role in M2 macrophage polarization and pro-tumoral factors production. The inhibition in M2-like TAM polarization caused by FBXW7 occurs through mediating c-Myc degradation via the ubiquitin-proteasome system, by the attachment of K48 poly-ubiquitin chains to c-Myc.

The E3 ligase FBXW7 is a known tumor suppressor. FBXW7 deletion in tumor cells determines the fate of tumor cells through limiting oncoprotein ubiquitin-mediated proteolysis and promoting their aberrant accumulation. FBXW7 also plays a pivotal role in tumorigenesis suppression through other manners. FBXW7 controls stem cells quiescence, self-renewal, and differentiation to influence tumorigenesis [57–60]. FBXW7 knockout in mouse embryonic fibroblasts induces the epithelial-to-mesenchymal transition to promote tumor metastasis [26]. FBXW7 mutations in BMSCs can increase the production of CCL2 to recruit immunosuppressive cells and promote metastasis [27]. We have now demonstrated a new function of FBXW7 in tumorigenesis suppression. FBXW7 depletion in myeloid cells could promote tumor growth. After subcutaneous injection with LLCs, $Lysm^{+}FBXW7^{f/f}$ mice had a higher death rate and larger tumor volumes compared to their wild-type littermates. Moreover, these differences were related to an increase in the proportion of $CD206^{+}$ TAMs caused by FBXW7 knockout in tumor tissues.

Cytokines, chemokines, and other mediators produced by M2-like TAMs regulate the immune suppressive microenvironment and modify the tumor micro-environment to facilitate cancer initiation, metastasis, and development [40, 42–44, 61, 62]. As one of the critical determinants in various cellular processes, the role of ubiquitination in macrophage polarization should be recognized. The E3 ligase Trim24 can catalyze acetyltransferase CREB-binding protein (CBP) ubiquitination to facilitate CBP-mediated acetylation of STAT6 to inhibit M2 macrophage polarization [63]. In the present study, we demonstrate that the E3 ligase FBXW7 is a novel mediator of M2 macrophage polarization. We observed that the expression of M2-associated proteins increased in primary macrophages derived from $Lysm^{+}FBXW7^{f/f}$ mice upon stimulation with LLC supernatant or IL-4. Furthermore, FBXW7 knockout promoted increased expression of cancer-promoting factors by M2-like TAMs. The percentage of M2-like TAMs infiltrated in tumor tissues in $Lysm^{+}FBXW7^{f/f}$ tumor-bearing mice was increased, accompanied with exacerbated tumor growth and a poor prognosis. In addition, Mice co-injected with LLCs and FBXW7-knockout M2 macrophages displayed more severe tumor progression.

c-Myc is a transcription factor that regulates several key signaling pathways involved in cellular growth and proliferation [51]. c-Myc can promote immuno-suppression as well as enhance adaptive immune response [64–68]. In the innate immune response, c-Myc plays a role in M2 macrophage polarization. The increased expression of c-Myc has previously been observed in M2 macrophages, and c-Myc can directly interact with the promoters of M2 macrophage-associated genes [50]. Since c-Myc is a downstream effector of multiple signaling pathways, its expression and activity are also controlled by other upstream signaling pathways, which subsequently controls activation and subtype differentiation of the macrophages [69, 70]. In previous studies, FBXW7 has been proven to catalyze the K48-linked ubiquitination of c-Myc, resulting in its degradation, thus regulating the stability of c-Myc to influence cell proliferation and tumorigenesis [54–56].

According to our data, c-Myc expression increased in LLC supernatant-induced macrophages, and this increase in c-Myc expression was affected to some extent by FBXW7. As the incubation time of the LLC supernatant increased, reduced FBXW7 expression attenuated its interaction and ubiquitination of c-Myc, increasing the stability and accumulation of c-Myc, and promoting M2-related gene expression, leading to M2-like TAM polarization. However, in late stages, FBXW7 gradually increased to restore the regulation of

c-Myc and prevent excessive or abnormal M2 macrophage polarization. When FBXW7 expression was abrogated, its function in limiting M2 macrophage polarization was abolished, increasing the number of aberrant M2-like TAMs that can promote cancer development.

While our work identified a novel role of FBXW7 in suppressing tumor growth, there are still notable questions that remain to be addressed. In a previous study, FBXW7 mutations in BMSCs, but not in macrophages, were found to be major contributors to the increased production of CCL2 leading to metastasis [27]. Interestingly, while the size of metastasized tumor nodules was reduced by treatment with a CCR2 antagonist, the number of tumor nodules was not affected [27]. This suggests that FBXW7 deficiency in bone marrow cells, including macrophages, MDSCs, and dendritic cells, may be involved in different stages of cancer development and might regulate tumor growth and metastasis through different mechanisms. Our previous study shows that FBXW7 mutations in macrophages may alleviate lung metastasis of murine melanoma, but the detailed mechanisms underlying these results remain unknown [71]. This also suggests that FBXW7 may affect tumor growth and metastasis through different mechanisms via macrophages. Considered that the same molecule or its isoforms may play a different regulatory role in macrophage activation states, several isoforms of FBXW7 may play different regulatory roles during macrophage differentiation and tumor progression. [25, 69, 72–74]. In addition, while the contribution of M2 macrophages has been well identified in tumor progression, the role of M1 macrophages in tumor remains controversial [75–78]. Clarifying the roles of different macrophage subset during cancer progression and at different stages is needed in future works. Additional experiments are required to elucidate the above problems.

In summary, our work demonstrates that FBXW7 mediates c-Myc K48-linked ubiquitination to limit the accumulation of c-Myc, leading to the inhibition of M2-like TAM polarization, thereby exerting a tumor-suppressive effect. These findings improve our understanding of the function of FBXW7 in macrophage plasticity and how it influences cancer development through non-malignant cells.

MATERIALS AND METHODS

Antibodies and reagents

For a list of antibodies and reagents used, see Supplementary Table 1.

Mice

$FBXW7^{f/f}$ mice on a C57BL/6J background were purchased from Jackson Laboratories. Lysm-Cre mice C57BL/6J were kindly provided by Dr. Ximei Wu, Zhejiang University School of Medicine. $Lysm^{+}FBXW7^{f/f}$ C57BL/6J mice were generated as we previously described [29]. C57BL/6J mice (6-8 weeks old) were purchased from the Model Animal Research Center of Nanjing University (Nanjing, China). All mice were bred with standard diet and kept at the University Laboratory Animal Center in a specific-pathogen-free environment and used at 6-10 weeks of age. All animal experiments were approved by the Animal Ethics Committee of Zhejiang University in compliance with institutional guidelines.

Cell culture

LLCs were purchased from the Cell Bank of the Chinese Academy of Science, Shanghai, China, and cultured in Dulbecco's modified Eagle's medium (DMEM) with 10% fetal bovine serum (FBS). Mouse peritoneal macrophages were induced by thioglycolate (Merck, Darmstadt, Germany) and extracted by peritoneal lavage. The cells were cultured in RPMI-1640 with 10% FBS. Bone marrow-derived macrophages (BMDMs) were extracted from mice femurs and cultured in RPMI-1640 with 10% FBS supplemented with recombinant mouse macrophage colony-stimulating factor (20 ng/mL).

For cell stimulation, peritoneal macrophages and BMDMs were treated with IL-4 (20 ng/ml) or conditioned medium containing LLC supernatant for the indicated time periods. Conditioned media were prepared as described previously [4].

Tumor model

Tumors were induced by injecting 1×10^6 LLCs in 100 μl PBS subcutaneously into the right flanks of 8-10-week-old mice. The mice were anesthetized and sacrificed on day 16 or when the largest diameter of the tumor exceeded 20 mm. Tumors were measured with calipers and removed for further experiments. To analyze the survival of tumor-induced mice, 3×10^5 LLCs in 100 μl PBS were injected subcutaneously into the right flanks of 8–10-week-old mice. For the co-injection model, as described previously [79], IL-4-induced M2 macrophages derived from $FBXW7^{f/f}$ or $Lysm^{+}FBXW7^{f/f}$ mice were mixed with LLCs at a ratio of 1:1. Then, 2×10^6 mixed cells in 200 μl PBS were co-injected subcutaneously into 6–8-week-old healthy wild-type C57BL/6 mice. The tumor volume (mm3) was calculated as following formula: volume = 0.5 x length x $width^2$.

Neutrophil depletion

As described previously [80], we injected 5.5 μg/g rat IgG2a isotype control antibody or 5.5 μg/g anti-Ly6G antibody intraperitoneally for 24 h prior to inoculating LLC cells. This was repeated every 3 days throughout the study. Collected blood samples from mice tail vein and analyzed the proportion of neutrophils to evaluate the efficiency of neutrophil depletion.

Flow cytometry analysis

Single-cell suspensions from tumors were prepared as described previously [81]. Briefly, the tumors were minced with scissors and digested in serum-free RPMI-1640 supplemented with Liberase (50 μg/ml) and DNase I (1 μg/ml) at 37 °C for 30 min. The single-cell suspensions were obtained through filtering, removing red blood cells, and washing with PBS after digestion. The prepared single-cell suspensions were then stained with the indicated antibodies and analyzed by flow cytometry.

Immunohistochemistry

Tumor tissues were fixed in 10% phosphate-buffered formalin, embedded in paraffin, sectioned, and stained with the corresponding antibodies according to the manufacturers' protocols.

Quantitative reverse transcriptase PCR

Total RNA was isolated from cells or tissues using Trizol reagent (Takara Bio, Shiga, Japan) and reverse transcribed to cDNA using ReverTra Ace (Toyobo, Osaka, Japan). For quantitative PCR (qPCR), cDNA fragments were amplified with the SYBR Green master Rox kit (Takara Bio). All protocols were performed in accordance with the manufacturers' protocols. The primer sequences used are shown in Supplementary Table 2 and Supplementary Table 3.

ELISA assay

Macrophages and tumor cells were co-cultured in Transwell chambers with 8-μm membrane pores in a 24-well plate in serum-free RPMI-1640 medium for indicated times. Collected macrophage supernatant and detected the cytokines expression using ELISA kits according to the manufacturer's instructions.

Co-immunoprecipitation and immunoblot analysis

For co-immunoprecipitation, cells were collected and lysed with IP Lysis Buffer (Pierce Biotechnology, Waltham, MA, USA) supplemented with protease inhibitor for 30 min at 4 °C. Cell lysates were centrifuged for 10 min at 12,000 × *g*, and the supernatants of the centrifuged cell lysates were incubated with specific antibodies bound to protein G magnetic beads overnight at 4°C. Then, the beads were washed three times with IP washing buffer and eluted with SDS loading buffer. Finally, equal amounts of eluted immunoprecipitants were subjected to immunoblot analysis.

Western blotting

The cells were lysed with cell lysis buffer (Cell Signaling Technology) supplemented with protease inhibitor. The concentration of supernatants from the centrifuged cell lysates were measured using the bicinchoninic acid (BCA) assay. Equal amounts of each protein sample were subjected to SDS-PAGE and electrically transferred to a polyvinylidene fluoride membrane (Millipore, Billerica, MA, USA). Immunoblots were incubated with the corresponding antibodies, as described above. Protein bands were visualized using the Pierce enhanced chemiluminescence (ECL) kit and then visualized and quantified using the Image J software.

MTT assay

Briefly, LLCs (3×10^3/well) were plated in 96-well plates and incubated in serum-free RPMI-1640 for 24 h. Then, the cells were stimulated with supernatant collected from M2 macrophages for the indicated time periods, prior to the addition of 10 μl MTT reagent to each well and incubation for 4 h. Next, 100 μl DMSO was added to each well and the plates were incubated with shaking for 10 min. The optical density value was detected using a Model 680 microplate reader (Bio-Rad Laboratories, Hercules, CA, USA).

Cell transfection

siRNAs were designed for *c-Myc* and *FBXW7* gene knockdown. Both siRNAs were produced by GenePharma (Shanghai, China). The sequences used are shown in Supplementary Table 1. Cells were transfected with the indicated siRNAs using Lipofectamine RNAiMAX Reagent (Invitrogen, Carlsbad, CA, USA) according the manufacturer's protocol. The knockdown efficiency of siRNAs was tested by western blot analysis.

Statistical analysis

All data were analyzed by GraphPad Prism 8 software. All data are shown as the mean ± SEM or mean ± SD. A two-tailed, unpaired Student's *t*-test was used for

comparisons between two groups, and two-way ANOVA was used for multiple comparisons. The log-rank (Mantel-Cox) test was used to determine statistical significance in the mouse survival study. A value of $P < 0.05$ was considered statistically significant.

AUTHOR CONTRIBUTIONS

LZ, YZ and ML performed experiments and data analysis. LZ, QW, ZC designed experiments. LZ wrote the manuscript. QW and ZC helped with manuscript editing. QW, ZC, YZ provided reagents and mice. DL and YS helped with mice experiments and related analysis.

ACKNOWLEDGMENTS

We thank Prof. Ximei Wu for providing the Lysm-Cre mice. We thank Zhenlu Chong, PhD and Yue Xue, PhD for critical reading of this manuscript. We thank the Key Laboratory of Immunity and Inflammatory Diseases of Zhejiang Province for technical support. We thank Editage (http://www.editage.cn) and English Edit OT (http://eeot.oncotarget.com/) for English language editing.

CONFLICTS OF INTEREST

The authors have declared that no conflicts of interest exist.

FUNDING

This work was supported by the National Natural Science Foundation of China (81870023, 81930041, 31870907), Natural Science Foundation of Zhejiang Province (LY17H100004, LZ19H100001).

REFERENCES

1. Biswas SK, Mantovani A. Macrophage plasticity and interaction with lymphocyte subsets: cancer as a paradigm. Nat Immunol. 2010; 11:889–96. https://doi.org/10.1038/ni.1937 PMID:20856220

2. Di Caro G, Cortese N, Castino GF, Grizzi F, Gavazzi F, Ridolfi C, Capretti G, Mineri R, Todoric J, Zerbi A, Allavena P, Mantovani A, Marchesi F. Dual prognostic significance of tumour-associated macrophages in human pancreatic adenocarcinoma treated or untreated with chemotherapy. Gut. 2016; 65:1710–20. https://doi.org/10.1136/gutjnl-2015-309193 PMID:26156960

3. Murray PJ. Macrophage polarization. Annu Rev Physiol. 2017; 79:541–66. https://doi.org/10.1146/annurev-physiol-022516-034339 PMID:27813830

4. Colegio OR, Chu NQ, Szabo AL, Chu T, Rhebergen AM, Jairam V, Cyrus N, Brokowski CE, Eisenbarth SC, Phillips GM, Cline GW, Phillips AJ, Medzhitov R. Functional polarization of tumour-associated macrophages by tumour-derived lactic acid. Nature. 2014; 513:559–63. https://doi.org/10.1038/nature13490 PMID:25043024

5. Casazza A, Laoui D, Wenes M, Rizzolio S, Bassani N, Mambretti M, Deschoemaeker S, Van Ginderachter JA, Tamagnone L, Mazzone M. Impeding macrophage entry into hypoxic tumor areas by Sema3A/Nrp1 signaling blockade inhibits angiogenesis and restores antitumor immunity. Cancer Cell. 2013; 24:695–709. https://doi.org/10.1016/j.ccr.2013.11.007 PMID:24332039

6. Celus W, Di Conza G, Oliveira AI, Ehling M, Costa BM, Wenes M, Mazzone M. Loss of caveolin-1 in metastasis-associated macrophages drives lung metastatic growth through increased angiogenesis. Cell Rep. 2017; 21:2842–54. https://doi.org/10.1016/j.celrep.2017.11.034 PMID:29212030

7. Ding X, Yang DR, Xia L, Chen B, Yu S, Niu Y, Wang M, Li G, Chang C. Targeting TR4 nuclear receptor suppresses prostate cancer invasion via reduction of infiltrating macrophages with alteration of the TIMP-1/MMP2/MMP9 signals. Mol Cancer. 2015; 14:16. https://doi.org/10.1186/s12943-014-0281-1 PMID:25623427

8. Han Y, Guo W, Ren T, Huang Y, Wang S, Liu K, Zheng B, Yang K, Zhang H, Liang X. Tumor-associated macrophages promote lung metastasis and induce epithelial-mesenchymal transition in osteosarcoma by activating the COX-2/STAT3 axis. Cancer Lett. 2019; 440:116–25. https://doi.org/10.1016/j.canlet.2018.10.011 PMID:30343113

9. Hughes R, Qian BZ, Rowan C, Muthana M, Keklikoglou I, Olson OC, Tazzyman S, Danson S, Addison C, Clemons M, Gonzalez-Angulo AM, Joyce JA, De Palma M, et al. Perivascular M2 macrophages stimulate tumor relapse after chemotherapy. Cancer Res. 2015; 75:3479–91. https://doi.org/10.1158/0008-5472.CAN-14-3587 PMID:26269531

10. Vinnakota K, Zhang Y, Selvanesan BC, Topi G, Salim T, Sand-Dejmek J, Jönsson G, Sjölander A. M2-like macrophages induce colon cancer cell invasion via matrix metalloproteinases. J Cell Physiol. 2017; 232:3468–80. https://doi.org/10.1002/jcp.25808 PMID:28098359

11. Gordon SR, Maute RL, Dulken BW, Hutter G, George BM, McCracken MN, Gupta R, Tsai JM, Sinha R, Corey D, Ring AM, Connolly AJ, Weissman IL. PD-1 expression by tumour-associated macrophages inhibits phagocytosis and tumour immunity. Nature. 2017; 545:495–99. https://doi.org/10.1038/nature22396 PMID:28514441

12. Kryczek I, Zou L, Rodriguez P, Zhu G, Wei S, Mottram P, Brumlik M, Cheng P, Curiel T, Myers L, Lackner A, Alvarez X, Ochoa A, et al. B7-H4 expression identifies a novel suppressive macrophage population in human ovarian carcinoma. J Exp Med. 2006; 203:871–81. https://doi.org/10.1084/jem.20050930 PMID:16606666

13. Ley S, Weigert A, Weichand B, Henke N, Mille-Baker B, Janssen RA, Brüne B. The role of TRKA signaling in IL-10 production by apoptotic tumor cell-activated macrophages. Oncogene. 2013; 32:631–40. https://doi.org/10.1038/onc.2012.77 PMID:22410777

14. Pollari M, Brück O, Pellinen T, Vähämurto P, Karjalainen-Lindsberg ML, Mannisto S, Kallioniemi O, Kellokumpu-Lehtinen PL, Mustjoki S, Leivonen SK, Leppä S. PD-L1^{+} tumor-associated macrophages and PD-1^{+} tumor-infiltrating lymphocytes predict survival in primary testicular lymphoma. Haematologica. 2018; 103:1908–14. https://doi.org/10.3324/haematol.2018.197194 PMID:30026337

15. Ngambenjawong C, Gustafson HH, Pun SH. Progress in tumor-associated macrophage (TAM)-targeted therapeutics. Adv Drug Deliv Rev. 2017; 114:206–21. https://doi.org/10.1016/j.addr.2017.04.010 PMID:28449873

16. Komohara Y, Fujiwara Y, Ohnishi K, Takeya M. Tumor-associated macrophages: potential therapeutic targets for anti-cancer therapy. Adv Drug Deliv Rev. 2016; 99:180–85. https://doi.org/10.1016/j.addr.2015.11.009 PMID:26621196

17. Hao Z, Sheng Y, Duncan GS, Li WY, Dominguez C, Sylvester J, Su YW, Lin GH, Snow BE, Brenner D, You-Ten A, Haight J, Inoue S, et al. K48-linked KLF4 ubiquitination by E3 ligase mule controls t-cell proliferation and cell cycle progression. Nat Commun. 2017; 8:14003. https://doi.org/10.1038/ncomms14003 PMID:28084302

18. Silmon de Monerri NC, Yakubu RR, Chen AL, Bradley PJ, Nieves E, Weiss LM, Kim K. The ubiquitin proteome of toxoplasma gondii reveals roles for protein ubiquitination in cell-cycle transitions. Cell Host Microbe. 2015; 18:621–33. https://doi.org/10.1016/j.chom.2015.10.014 PMID:26567513

19. Hu B, Li S, Zhang X, Zheng X. HSCARG, a novel regulator of H2A ubiquitination by downregulating PRC1 ubiquitin E3 ligase activity, is essential for cell proliferation. Nucleic Acids Res. 2014; 42:5582–93. https://doi.org/10.1093/nar/gku230 PMID:24711370

20. Jiang X, Chen ZJ. The role of ubiquitylation in immune defence and pathogen evasion. Nat Rev Immunol. 2011; 12:35–48. https://doi.org/10.1038/nri3111 PMID:22158412

21. Wang H, Meng H, Li X, Zhu K, Dong K, Mookhtiar AK, Wei H, Li Y, Sun SC, Yuan J. PELI1 functions as a dual modulator of necroptosis and apoptosis by regulating ubiquitination of RIPK1 and mRNA levels of c-FLIP. Proc Natl Acad Sci USA. 2017; 114:11944–49. https://doi.org/10.1073/pnas.1715742114 PMID:29078411

22. Zheng N, Shabek N. Ubiquitin ligases: structure, function, and regulation. Annu Rev Biochem. 2017; 86:129–57. https://doi.org/10.1146/annurev-biochem-060815-014922 PMID:28375744

23. Goru SK, Pandey A, Gaikwad AB. E3 ubiquitin ligases as novel targets for inflammatory diseases. Pharmacol Res. 2016; 106:1–9. https://doi.org/10.1016/j.phrs.2016.02.006 PMID:26875639

24. Yeh CH, Bellon M, Nicot C. FBXW7: a critical tumor suppressor of human cancers. Mol Cancer. 2018; 17:115. https://doi.org/10.1186/s12943-018-0857-2 PMID:30086763

25. Welcker M, Clurman BE. FBW7 ubiquitin ligase: a tumour suppressor at the crossroads of cell division, growth and differentiation. Nat Rev Cancer. 2008; 8:83–93. https://doi.org/10.1038/nrc2290 PMID:18094723

26. Zhang Y, Zhang X, Ye M, Jing P, Xiong J, Han Z, Kong J, Li M, Lai X, Chang N, Zhang J, Zhang J. FBW7 loss promotes epithelial-to-mesenchymal transition in non-small cell lung cancer through the stabilization of snail protein. Cancer Lett. 2018; 419:75–83. https://doi.org/10.1016/j.canlet.2018.01.047 PMID:29355657

27. Yumimoto K, Akiyoshi S, Ueo H, Sagara Y, Onoyama I, Ueo H, Ohno S, Mori M, Mimori K, Nakayama KI. F-box protein FBXW7 inhibits cancer metastasis in a non-cell-autonomous manner. J Clin Invest. 2015; 125:621–35. https://doi.org/10.1172/JCI78782 PMID:25555218

28. Balamurugan K, Sharan S, Klarmann KD, Zhang Y, Coppola V, Summers GH, Roger T, Morrison DK, Keller JR, Sterneck E. FBXW7α attenuates inflammatory signalling by downregulating C/EBPδ and its target gene Tlr4. Nat Commun. 2013; 4:1662. https://doi.org/10.1038/ncomms2677 PMID:23575666

29. Song Y, Lai L, Chong Z, He J, Zhang Y, Xue Y, Xie Y, Chen S, Dong P, Chen L, Chen Z, Dai F, Wan X, et al. E3 ligase FBXW7 is critical for RIG-I stabilization during antiviral responses. Nat Commun. 2017; 8:14654. https://doi.org/10.1038/ncomms14654 PMID:28287082

30. Akhoondi S, Sun D, von der Lehr N, Apostolidou S, Klotz K, Maljukova A, Cepeda D, Fiegl H, Dafou D, Marth C, Mueller-Holzner E, Corcoran M, Dagnell M, et al. FBXW7/hCDC4 is a general tumor suppressor in human cancer. Cancer Res. 2007; 67:9006–12. https://doi.org/10.1158/0008-5472.CAN-07-1320 PMID:17909001

31. Altorki NK, Markowitz GJ, Gao D, Port JL, Saxena A, Stiles B, McGraw T, Mittal V. The lung microenvironment: an important regulator of tumour growth and metastasis. Nat Rev Cancer. 2019; 19:9–31. https://doi.org/10.1038/s41568-018-0081-9 PMID:30532012

32. Binnewies M, Roberts EW, Kersten K, Chan V, Fearon DF, Merad M, Coussens LM, Gabrilovich DI, Ostrand-Rosenberg S, Hedrick CC, Vonderheide RH, Pittet MJ, Jain RK, et al. Understanding the tumor immune microenvironment (TIME) for effective therapy. Nat Med. 2018; 24:541–50. https://doi.org/10.1038/s41591-018-0014-x PMID:29686425

33. Engblom C, Pfirschke C, Pittet MJ. The role of myeloid cells in cancer therapies. Nat Rev Cancer. 2016; 16:447–62. https://doi.org/10.1038/nrc.2016.54 PMID:27339708

34. Quail DF, Joyce JA. Microenvironmental regulation of tumor progression and metastasis. Nat Med. 2013; 19:1423–37. https://doi.org/10.1038/nm.3394 PMID:24202395

35. De Palma M, Lewis CE. Macrophage regulation of tumor responses to anticancer therapies. Cancer Cell. 2013; 23:277–86. https://doi.org/10.1016/j.ccr.2013.02.013 PMID:23518347

36. Burger JA, Wiestner A. Targeting B cell receptor signalling in cancer: preclinical and clinical advances. Nat Rev Cancer. 2018; 18:148–67. https://doi.org/10.1038/nrc.2017.121 PMID:29348577

37. Fesnak AD, June CH, Levine BL. Engineered T cells: the promise and challenges of cancer immunotherapy. Nat Rev Cancer. 2016; 16:566–81. https://doi.org/10.1038/nrc.2016.97 PMID:27550819

38. He J, Song Y, Li G, Xiao P, Liu Y, Xue Y, Cao Q, Tu X, Pan T, Jiang Z, Cao X, Lai L, Wang Q. Fbxw7 increases CCL2/7 in CX3CR1hi macrophages to promote intestinal inflammation. J Clin Invest. 2019; 129:3877–93. https://doi.org/10.1172/JCI123374 PMID:31246581

39. Lewis JS, Landers RJ, Underwood JCE, Harris AL, Lewis CE. Expression of vascular endothelial growth factor by macrophages is up-regulated in poorly vascularized areas of breast carcinomas. J Pathol. 2000; 192:150–8. https://doi.org/10.1002/1096-9896(2000)9999:9999<::AID-PATH687>3.0.CO;2-G

40. Verma S, Kesh K, Gupta A, Swarnakar S. An overview of matrix metalloproteinase 9 polymorphism and gastric cancer risk. Asian Pac J Cancer Prev. 2015; 16:7393–400. https://doi.org/10.7314/apjcp.2015.16.17.7393 PMID:26625734

41. Locati M, Curtale G, Mantovani A. Diversity, mechanisms, and significance of macrophage plasticity. Annu Rev Pathol. 2020; 15:123–47. https://doi.org/10.1146/annurev-pathmechdis-012418-012718 PMID:31530089

42. Harney AS, Arwert EN, Entenberg D, Wang Y, Guo P, Qian BZ, Oktay MH, Pollard JW, Jones JG, Condeelis JS. Real-time imaging reveals local, transient vascular permeability, and tumor cell intravasation stimulated by TIE2hi macrophage-derived VEGFA. Cancer Discov. 2015; 5:932–43. https://doi.org/10.1158/2159-8290.CD-15-0012 PMID:26269515

43. Lin EY, Pollard JW. Tumor-associated macrophages press the angiogenic switch in breast cancer. Cancer Res. 2007; 67:5064–66. https://doi.org/10.1158/0008-5472.CAN-07-0912 PMID:17545580

44. Oft M. IL-10: master switch from tumor-promoting inflammation to antitumor immunity. Cancer Immunol Res. 2014; 2:194–99. https://doi.org/10.1158/2326-6066.CIR-13-0214 PMID:24778315

45. Cosín-Roger J, Ortiz-Masiá D, Calatayud S, Hernández C, Esplugues JV, Barrachina MD. The activation of Wnt signaling by a STAT6-dependent macrophage phenotype promotes mucosal repair in murine IBD. Mucosal Immunol. 2016; 9:986–98. https://doi.org/10.1038/mi.2015.123 PMID:26601901

46. Pello OM. Macrophages and c-myc cross paths. Oncoimmunology. 2016; 5:e1151991. https://doi.org/10.1080/2162402X.2016.1151991 PMID:27471623

47. Hao J, Hu Y, Li Y, Zhou Q, Lv X. Involvement of JNK signaling in IL4-induced M2 macrophage polarization. Exp Cell Res. 2017; 357:155–62. https://doi.org/10.1016/j.yexcr.2017.05.010 PMID:28501460

48. Shan M, Qin J, Jin F, Han X, Guan H, Li X, Zhang J, Zhang H, Wang Y. Autophagy suppresses isoprenaline-induced M2 macrophage polarization via the ROS/ERK and mTOR signaling pathway. Free Radic Biol Med. 2017; 110:432–43. https://doi.org/10.1016/j.freeradbiomed.2017.05.021 PMID:28647611

49. Zhang W, Xu W, Xiong S. Macrophage differentiation and polarization via phosphatidylinositol 3-kinase/Akt-ERK signaling pathway conferred by serum amyloid P component. J Immunol. 2011; 187:1764–77. https://doi.org/10.4049/jimmunol.1002315 PMID:21753147

50. Pello OM, De Pizzol M, Mirolo M, Soucek L, Zammataro L, Amabile A, Doni A, Nebuloni M, Swigart LB, Evan GI, Mantovani A, Locati M. Role of c-MYC in alternative activation of human macrophages and tumor-associated macrophage biology. Blood. 2012; 119:411–21. https://doi.org/10.1182/blood-2011-02-339911 PMID:22067385

51. Adhikary S, Eilers M. Transcriptional regulation and transformation by myc proteins. Nat Rev Mol Cell Biol. 2005; 6:635–45. https://doi.org/10.1038/nrm1703 PMID:16064138

52. Dang CV. MYC on the path to cancer. Cell. 2012; 149:22–35. https://doi.org/10.1016/j.cell.2012.03.003 PMID:22464321

53. Dang CV. MYC, metabolism, cell growth, and tumorigenesis. Cold Spring Harb Perspect Med. 2013; 3:a014217. https://doi.org/10.1101/cshperspect.a014217 PMID:23906881

54. Yada M, Hatakeyama S, Kamura T, Nishiyama M, Tsunematsu R, Imaki H, Ishida N, Okumura F, Nakayama K, Nakayama KI. Phosphorylation-dependent degradation of c-Myc is mediated by the F-box protein Fbw7. EMBO J. 2004; 23:2116–25. https://doi.org/10.1038/sj.emboj.7600217 PMID:15103331

55. King B, Trimarchi T, Reavie L, Xu L, Mullenders J, Ntziachristos P, Aranda-Orgilles B, Perez-Garcia A, Shi J, Vakoc C, Sandy P, Shen SS, Ferrando A, Aifantis I. The ubiquitin ligase FBXW7 modulates leukemia-initiating cell activity by regulating MYC stability. Cell. 2013; 153:1552–66. https://doi.org/10.1016/j.cell.2013.05.041 PMID:23791182

56. Popov N, Schülein C, Jaenicke LA, Eilers M. Ubiquitylation of the amino terminus of myc by SCF(β-TrCP) antagonizes SCF(Fbw7)-mediated turnover. Nat Cell Biol. 2010; 12:973–81. https://doi.org/10.1038/ncb2104 PMID:20852628

57. Reavie L, Della Gatta G, Crusio K, Aranda-Orgilles B, Buckley SM, Thompson B, Lee E, Gao J, Bredemeyer AL, Helmink BA, Zavadil J, Sleckman BP, Palomero T, et al. Regulation of hematopoietic stem cell differentiation by a single ubiquitin ligase-substrate complex. Nat Immunol. 2010; 11:207–15. https://doi.org/10.1038/ni.1839 PMID:20081848

58. Cremona CA, Sancho R, Diefenbacher ME, Behrens A. Fbw7 and its counteracting forces in stem cells and cancer: oncoproteins in the balance. Semin Cancer Biol. 2016; 36:52–61. https://doi.org/10.1016/j.semcancer.2015.09.006 PMID:26410034

59. Sancho R, Jandke A, Davis H, Diefenbacher ME, Tomlinson I, Behrens A. F-box and WD repeat domain-containing 7 regulates intestinal cell lineage commitment and is a haploinsufficient tumor suppressor. Gastroenterology. 2010; 139:929–41. https://doi.org/10.1053/j.gastro.2010.05.078 PMID:20638938

60. Thompson BJ, Jankovic V, Gao J, Buonamici S, Vest A, Lee JM, Zavadil J, Nimer SD, Aifantis I. Control of hematopoietic stem cell quiescence by the E3 ubiquitin ligase Fbw7. J Exp Med. 2008; 205:1395–408. https://doi.org/10.1084/jem.20080277 PMID:18474632

61. De Palma M, Biziato D, Petrova TV. Microenvironmental regulation of tumour angiogenesis. Nat Rev Cancer. 2017; 17:457–74. https://doi.org/10.1038/nrc.2017.51 PMID:28706266

62. Fu Q, Xu L, Wang Y, Jiang Q, Liu Z, Zhang J, Zhou Q, Zeng H, Tong S, Wang T, Qi Y, Hu B, Fu H, et al. Tumor-associated macrophage-derived interleukin-23 interlinks kidney cancer glutamine addiction with immune evasion. Eur Urol. 2019; 75:752–63. https://doi.org/10.1016/j.eururo.2018.09.030 PMID:30293904

63. Yu T, Gan S, Zhu Q, Dai D, Li N, Wang H, Chen X, Hou D, Wang Y, Pan Q, Xu J, Zhang X, Liu J, et al. Modulation of M2 macrophage polarization by the crosstalk between Stat6 and Trim24. Nat Commun. 2019; 10:4353.

https://doi.org/10.1038/s41467-019-12384-2
PMID:31554795

64. Calado DP, Sasaki Y, Godinho SA, Pellerin A, Köchert K, Sleckman BP, de Alborán IM, Janz M, Rodig S, Rajewsky K. The cell-cycle regulator c-Myc is essential for the formation and maintenance of germinal centers. Nat Immunol. 2012; 13:1092–100.
https://doi.org/10.1038/ni.2418
PMID:23001146

65. Casey SC, Tong L, Li Y, Do R, Walz S, Fitzgerald KN, Gouw AM, Baylot V, Gütgemann I, Eilers M, Felsher DW. MYC regulates the antitumor immune response through CD47 and PD-L1. Science. 2016; 352:227–31.
https://doi.org/10.1126/science.aac9935
PMID:26966191

66. Chou C, Pinto AK, Curtis JD, Persaud SP, Cella M, Lin CC, Edelson BT, Allen PM, Colonna M, Pearce EL, Diamond MS, Egawa T. c-Myc-induced transcription factor AP4 is required for host protection mediated by CD8+ T cells. Nat Immunol. 2014; 15:884–93.
https://doi.org/10.1038/ni.2943 PMID:25029552

67. Heinzel S, Binh Giang T, Kan A, Marchingo JM, Lye BK, Corcoran LM, Hodgkin PD. A Myc-dependent division timer complements a cell-death timer to regulate T cell and B cell responses. Nat Immunol. 2017; 18:96–103.
https://doi.org/10.1038/ni.3598 PMID:27820810

68. Wang R, Dillon CP, Shi LZ, Milasta S, Carter R, Finkelstein D, McCormick LL, Fitzgerald P, Chi H, Munger J, Green DR. The transcription factor Myc controls metabolic reprogramming upon T lymphocyte activation. Immunity. 2011; 35:871–82.
https://doi.org/10.1016/j.immuni.2011.09.021
PMID:22195744

69. Li L, Ng DS, Mah WC, Almeida FF, Rahmat SA, Rao VK, Leow SC, Laudisi F, Peh MT, Goh AM, Lim JS, Wright GD, Mortellaro A, et al. A unique role for p53 in the regulation of M2 macrophage polarization. Cell Death Differ. 2015; 22:1081–93.
https://doi.org/10.1038/cdd.2014.212
PMID:25526089

70. Yang Y, Ye YC, Chen Y, Zhao JL, Gao CC, Han H, Liu WC, Qin HY. Crosstalk between hepatic tumor cells and macrophages via Wnt/β-catenin signaling promotes M2-like macrophage polarization and reinforces tumor Malignant behaviors. Cell Death Dis. 2018; 9:793.
https://doi.org/10.1038/s41419-018-0818-0
PMID:30022048

71. Wei Z, Lihua L, Qingqing W. [Effects of myeloid specific deficiency of FBXW7 on lung metastasis of murine melanoma]. Zhejiang Da Xue Xue Bao Yi Xue Ban. 2017; 46:111–17.
PMID:28752701

72. Ye S, Xu H, Jin J, Yang M, Wang C, Yu Y, Cao X. The E3 ubiquitin ligase neuregulin receptor degradation protein 1 (Nrdp1) promotes M2 macrophage polarization by ubiquitinating and activating transcription factor CCAAT/enhancer-binding protein β (C/EBPβ). J Biol Chem. 2012; 287:26740–48.
https://doi.org/10.1074/jbc.M112.383265
PMID:22707723

73. Vergadi E, Ieronymaki E, Lyroni K, Vaporidi K, Tsatsanis C. Akt signaling pathway in macrophage activation and M1/M2 polarization. J Immunol. 2017; 198:1006–14.
https://doi.org/10.4049/jimmunol.1601515
PMID:28115590

74. Long Y, Zhu Y. Identification of FBXW7α-regulated genes in M1-polarized macrophages in colorectal cancer by RNA sequencing. Saudi Med J. 2019; 40:766–73.
https://doi.org/10.15537/smj.2019.8.24361
PMID:31423512

75. Dufresne M, Dumas G, Asselin E, Carrier C, Pouliot M, Reyes-Moreno C. Pro-inflammatory type-1 and anti-inflammatory type-2 macrophages differentially modulate cell survival and invasion of human bladder carcinoma T24 cells. Mol Immunol. 2011; 48:1556–67.
https://doi.org/10.1016/j.molimm.2011.04.022
PMID:21601924

76. Helm O, Held-Feindt J, Grage-Griebenow E, Reiling N, Ungefroren H, Vogel I, Krüger U, Becker T, Ebsen M, Röcken C, Kabelitz D, Schäfer H, Sebens S. Tumor-associated macrophages exhibit pro- and anti-inflammatory properties by which they impact on pancreatic tumorigenesis. Int J Cancer. 2014; 135:843–61.
https://doi.org/10.1002/ijc.28736
PMID:24458546

77. Wang H, Wang X, Li X, Fan Y, Li G, Guo C, Zhu F, Zhang L, Shi Y. CD68(+)HLA-DR(+) M1-like macrophages promote motility of HCC cells via NF-κB/FAK pathway. Cancer Lett. 2014; 345:91–99.
https://doi.org/10.1016/j.canlet.2013.11.013
PMID:24333724

78. Wu TH, Li YY, Wu TL, Chang JW, Chou WC, Hsieh LL, Chen JR, Yeh KY. Culture supernatants of different colon cancer cell lines induce specific phenotype switching and functional alteration of THP-1 cells. Cell Immunol. 2014; 290:107–15.
https://doi.org/10.1016/j.cellimm.2014.05.015
PMID:24960291

79. Tan B, Shi X, Zhang J, Qin J, Zhang N, Ren H, Qian M, Siwko S, Carmon K, Liu Q, Han H, Du B, Liu M. Inhibition of rspo-Lgr4 facilitates checkpoint blockade therapy by switching macrophage polarization. Cancer Res. 2018; 78:4929–42.

https://doi.org/10.1158/0008-5472.CAN-18-0152
PMID:29967265

80. García-Mendoza MG, Inman DR, Ponik SM, Jeffery JJ, Sheerar DS, Van Doorn RR, Keely PJ. Neutrophils drive accelerated tumor progression in the collagen-dense mammary tumor microenvironment. Breast Cancer Res. 2016; 18:49.
https://doi.org/10.1186/s13058-016-0703-7
PMID:27169366

`81. Li Q, Anderson CD, Egilmez NK. Inhaled IL-10 suppresses lung tumorigenesis via abrogation of inflammatory macrophage-Th17 cell axis. J Immunol. 2018; 201:2842–50.
https://doi.org/10.4049/jimmunol.1800141
PMID:30257887

SUPPLEMENTARY MATERIALS

Supplementary Figures

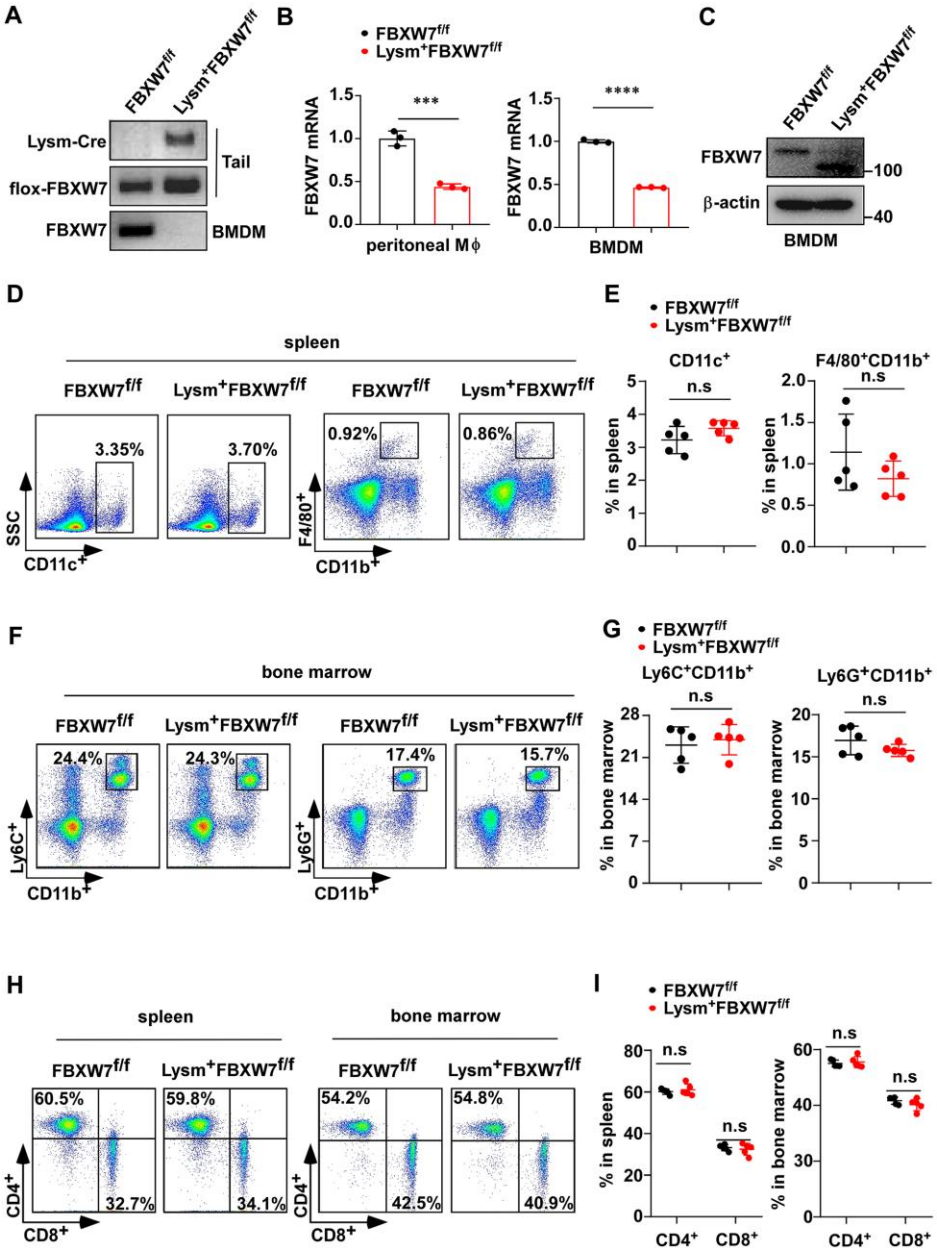

Supplementary Figure 1. FBXW7 knockout in myeloid cells does not affect the development of myeloid cells and lymphocytes. (**A**) PCR analysis "Lysm-Cre", "flox" sequences of FBXW7$^{f/f}$ and Lysm^{+}FBXW7$^{f/f}$ mice, PCR analysis the excision of exons 5 and 6 of FBXW7 in bone marrow-derived macrophages (BMDMs) from FBXW7$^{f/f}$ and Lysm^{+}FBXW7$^{f/f}$ mice. (**B**) qRT-PCR analysis of *FBXW7* expression in peritoneal macrophages and BMDMs derived from FBXW7$^{f/f}$ and Lysm^{+}FBXW7$^{f/f}$ mice. (**C**) Western blot analysis of FBXW7 expression in BMDMs derived from FBXW7$^{f/f}$ and Lysm^{+}FBXW7$^{f/f}$ mice. (**D, E**) Flow cytometry analysis (**D**) and statistical analysis (**E**) of CD11c^{+} dendritic cells and F4/80^{+}CD11b^{+} macrophages in the spleen of FBXW7$^{f/f}$ and Lysm^{+}FBXW7$^{f/f}$ mice (n=5 per group). (**F, G**) Flow cytometry analysis (**F**) and statistical analysis (**G**) of Ly6C^{+}CD11b^{+} monocytes and Ly6G^{+}CD11b^{+} granulocytes in the bone marrow of FBXW7$^{f/f}$ and Lysm^{+}FBXW7$^{f/f}$ mice (n=5 per group). (**H**) Flow cytometry analysis of CD4^{+} and CD8^{+} T cells in the spleen and bone marrow from FBXW7$^{f/f}$ and Lysm^{+}FBXW7$^{f/f}$ mice. (**I**) Statistical differences in the proportions of CD4^{+} and CD8^{+} T cells in the spleen and bone marrow of FBXW7$^{f/f}$ and Lysm^{+}FBXW7$^{f/f}$ mice by flow cytometry (n=5 per group). Data are shown as the mean ± SD and are representative of three independent experiments. n = 3 or 5. ***P < 0.001; ****P < 0.0001; n.s, no significance (Student's t test (**B**, **E**, **G**, **I**)).

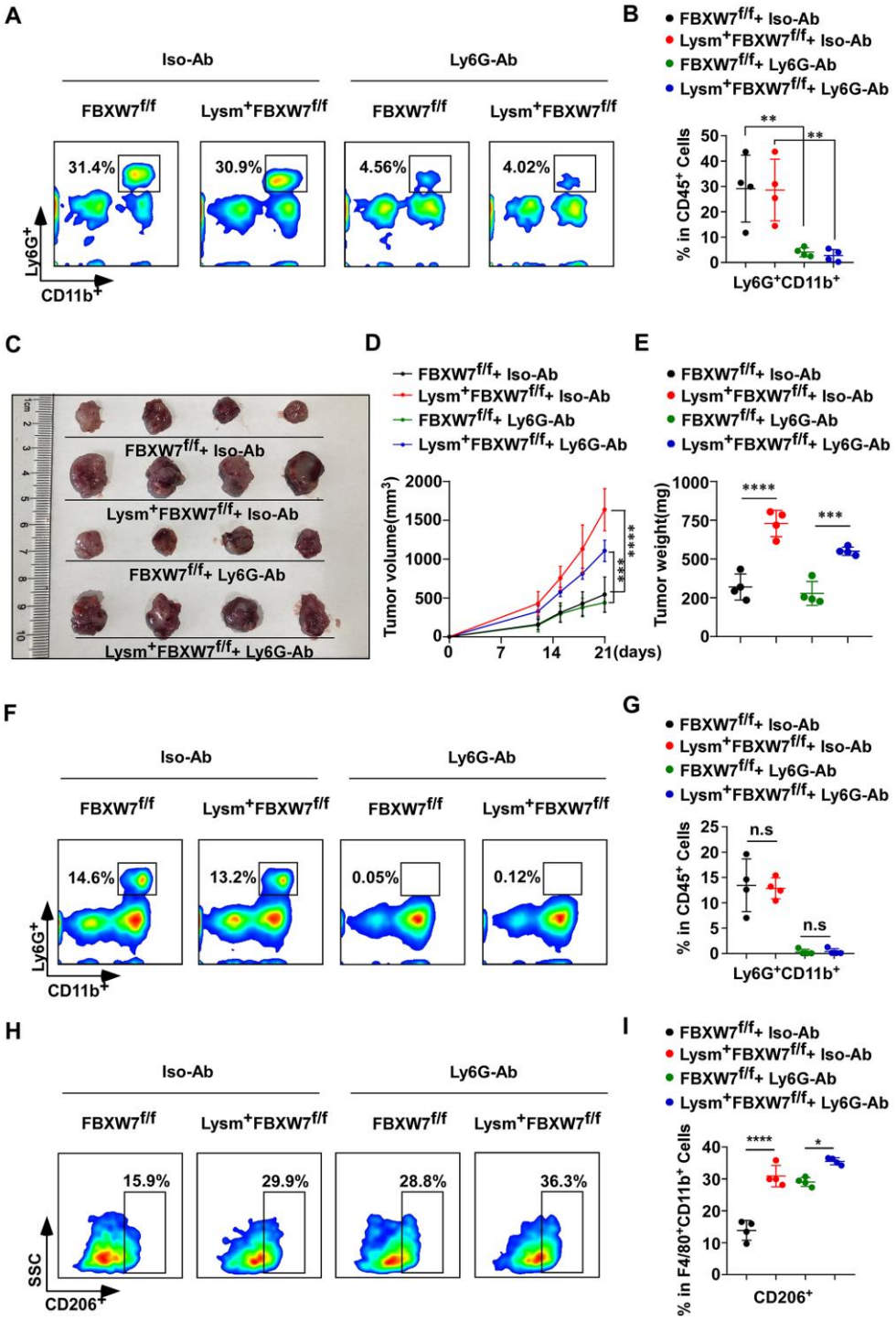

Supplementary Figure 2. Neutrophils are not responsible for the aggravated tumor progression in Lysm^{+}FBXW7$^{f/f}$ mice. (**A**, **B**) Neutrophils were depleted by anti-Ly6G mAb. Flow cytometry analysis (**A**) and statistical analysis (**B**) of the percentage of neutrophils (Ly6G^{+}CD11b^{+}) in the blood of FBXW7$^{f/f}$ and Lysm^{+}FBXW7$^{f/f}$ mice with or without anti-Ly6G mAb used showed to evaluate the efficiency of depletion. (n = 4 per group). (**C**–**E**) FBXW7$^{f/f}$ and Lysm^{+}FBXW7$^{f/f}$ mice inoculated with LLCs after anti-Ly6G mAb or isotype control antibody used. The appearance (**C**), volume (**D**), weight (**E**) of tumors in four groups in 21 days. (**F**, **G**) Flow cytometry analysis (**F**) and statistical analysis (**G**) of the percentage of neutrophils (Ly6G^{+}CD11b^{+}) in the tumors of FBXW7$^{f/f}$ and Lysm^{+}FBXW7$^{f/f}$ mice with or without anti-Ly6G mAb used (n = 4 per group). (**H**, **I**) Flow cytometry analysis (**H**) and statistical analysis (**I**) of the percentage of CD206^{+} macrophages in tumors of FBXW7$^{f/f}$ and Lysm^{+}FBXW7$^{f/f}$ mice with or without anti-Ly6G mAb used (n = 4 per group). *P < 0.05; **P < 0.01; ***P < 0.001; ****P < 0.0001; n.s, no significance (one-way ANOVA (**B**, **D**, **E**, **G**, **I**)).

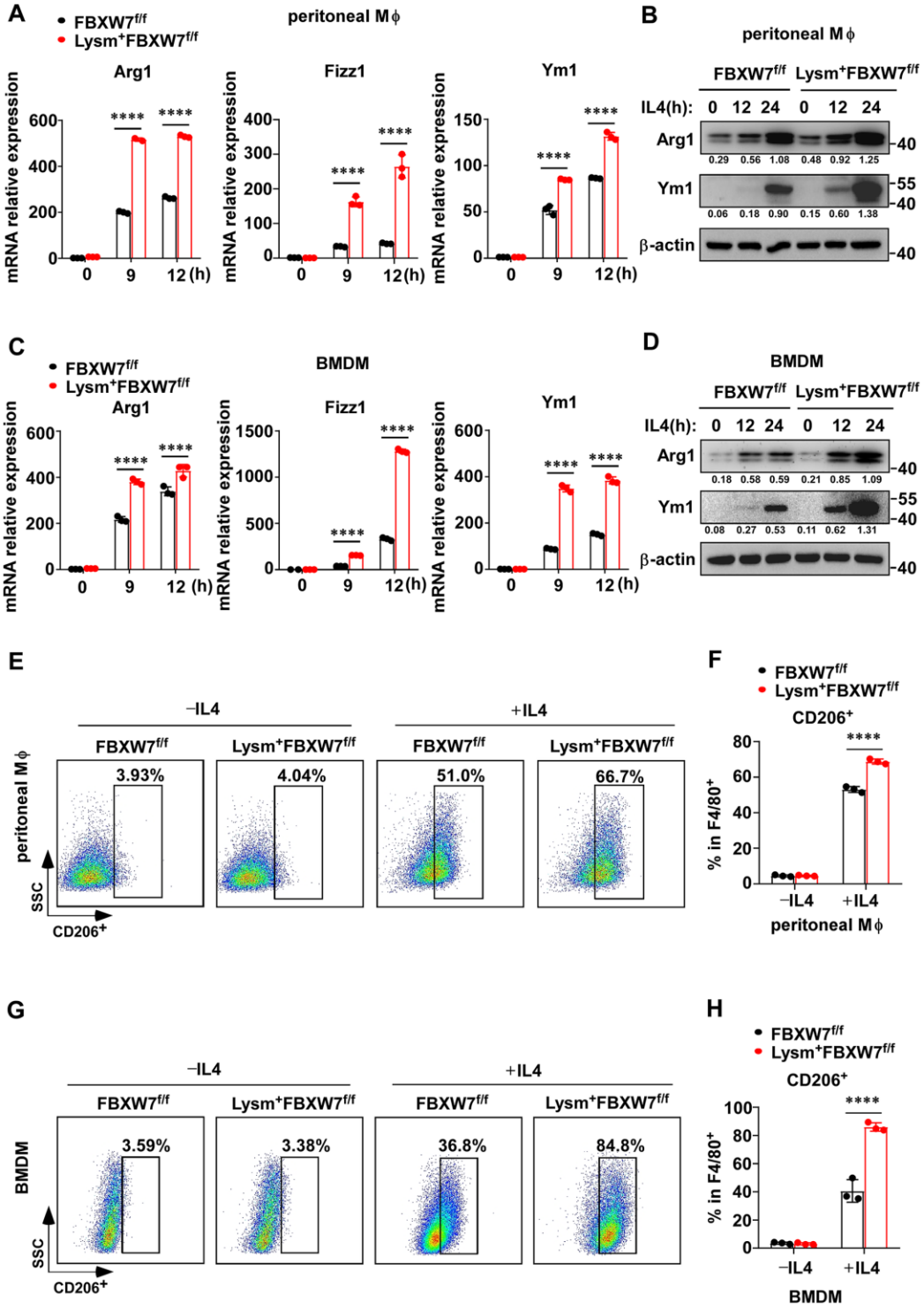

Supplementary Figure 3. FBXW7 knockout enhances IL-4-induced M2 macrophage polarization. (**A**) Peritoneal macrophages extracted from FBXW7$^{f/f}$ and Lysm^{+}FBXW7$^{f/f}$ mice were treated with IL-4 (20 ng/ml), and the mRNA expression of *Arg1*, *Fizz1*, and *Ym1* was analyzed by qRT-PCR. (**B**) The protein expression of Arg1 and Ym1 from wild-type and FBXW7-knockout peritoneal macrophages stimulated with IL-4 was detected by immunoblotting. (**C**, **D**) The mRNA (**C**) and protein (**D**) expression of M2-like TAM-associated genes were analyzed by qRT-PCR and immunoblotting, respectively, in BMDMs stimulated with IL-4. (**E**, **F**) Flow cytometry analysis (**E**) and statistical analysis (**F**) of the percentage of M2 macrophages (CD206^{+}) in wild-type and FBXW7-knockdown peritoneal macrophages after IL-4 stimulation for 24 h (n = 3 per group). (**G**, **H**) Flow cytometry analysis (**G**) and statistical analysis (**H**) of the percentage of M2 macrophages (CD206^{+}) in wild-type and FBXW7-knockout BMDMs after IL-4 stimulation for 24 h (n = 3 per group). Data are shown as the mean ± SD and are representative of three independent experiments. ***$P < 0.001$; ****$P < 0.0001$; n.s, no significance (two-way ANOVA (**A**, **C**, **F**, **H**)).

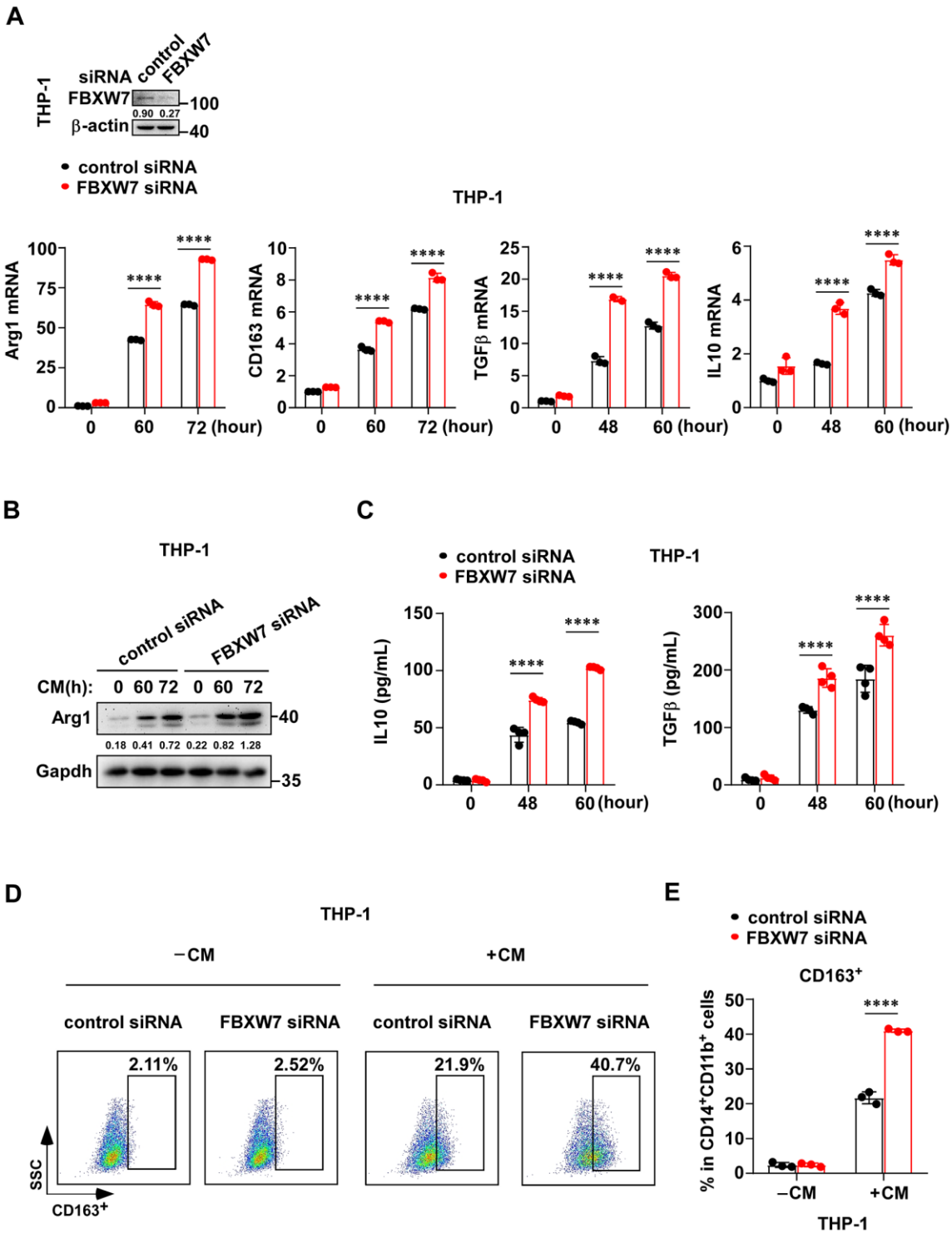

Supplementary Figure 4. FBXW7 knockdown in THP-1 promotes A549 supernatant-induced M2 macrophage polarization. (**A**) THP-1 cells were differentiated into macrophages in the presence of PMA for 48 hours and transfected with FBXW7 siRNA. The silenced and unsilenced THP-1 stimulated with conditioned medium containing A549 cells cultured supernatant. The protein expression of FBXW7 in THP-1 was examined by immunoblotting and the mRNA expression of *Arg1, CD163, TGFβ,* and *IL10* was detected by qRT-PCR. (**B**) The protein expression of Arg1 in two groups was examined by immunoblotting. (**C**) The protein levels of IL10 and TGFβ in the supernatant of wild-type and FBXW7-knockdown THP-1 that co-cultured with A549 cells for the indicated time were measured by ELISA kits. (**D**, **E**) Flow cytometry analysis (**D**) and statistical analysis (**E**) of the percentage of M2 macrophages ($CD163^+$) in wild-type and FBXW7-knockdown THP-1 after conditioned medium stimulation for 72 h (n = 3 per group). Data are shown as the mean ± SD and are representative of three independent experiments. ****$P < 0.0001$; (two-way ANOVA (**A**, **C**, **E**)).

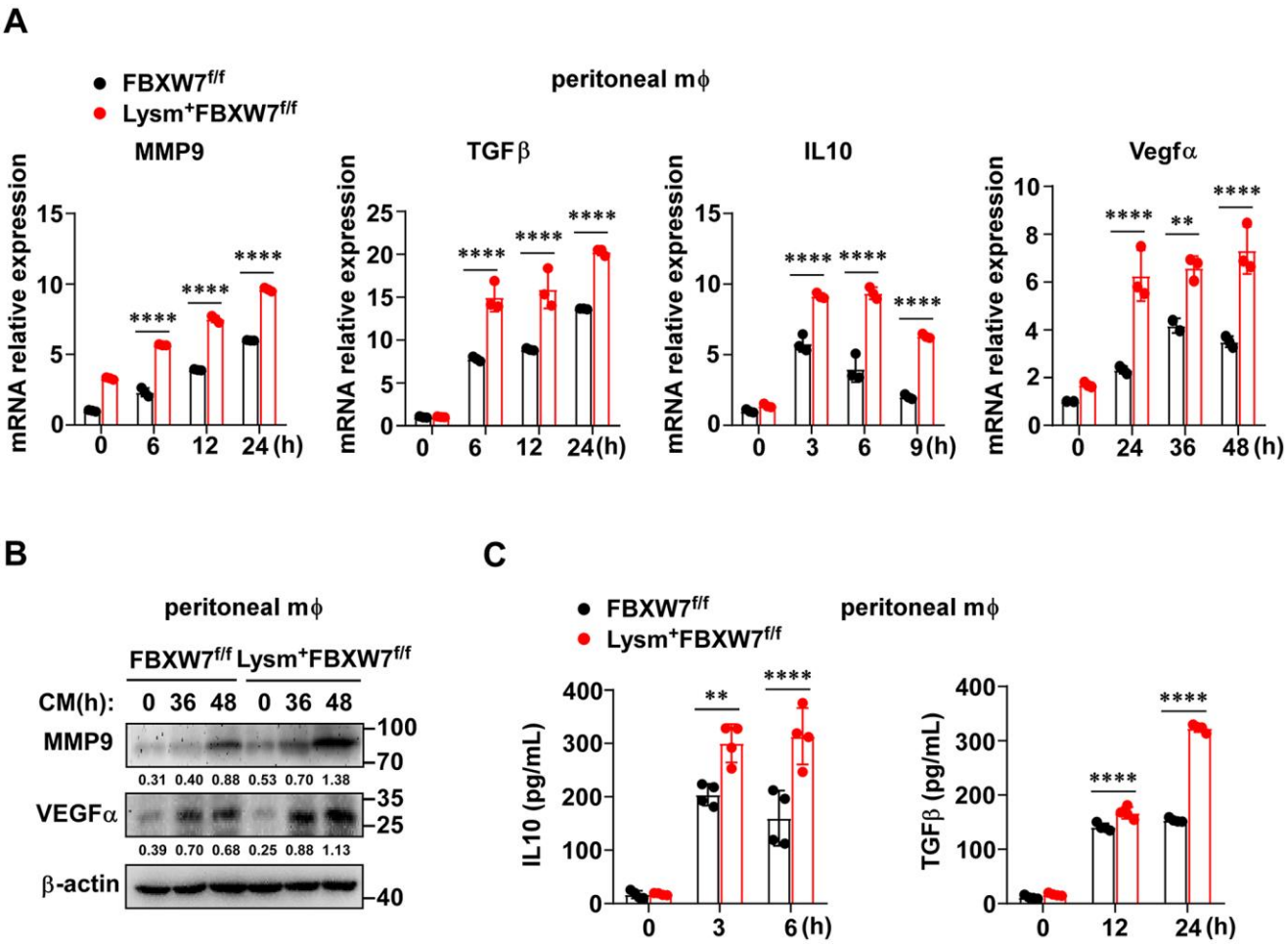

Supplementary Figure 5. FBXW7 knockout promotes the expression of pro-tumoral factors in peritoneal macrophages. (**A**) Peritoneal macrophages from FBXW7$^{f/f}$ and Lysm^{+}FBXW7$^{f/f}$ mice were stimulated with the conditioned medium, and the mRNA expression of *MMP9, IL-10, TGFβ,* and *VEGFα* was examined by qRT-PCR. (**B**) The protein expression of MMP9 and VEGFα in peritoneal macrophages incubated with the conditioned medium were detected by immunoblotting. (**C**) The protein levels of IL10 and TGFβ in the supernatant of peritoneal macrophages that co-cultured with LLCs for the indicated time was measured by ELISA kits. Data are shown as the mean ± SD and are representative of three independent experiments. ***P* < 0.01; *****P* < 0.0001 (two-way ANOVA (**A**, **C**)).

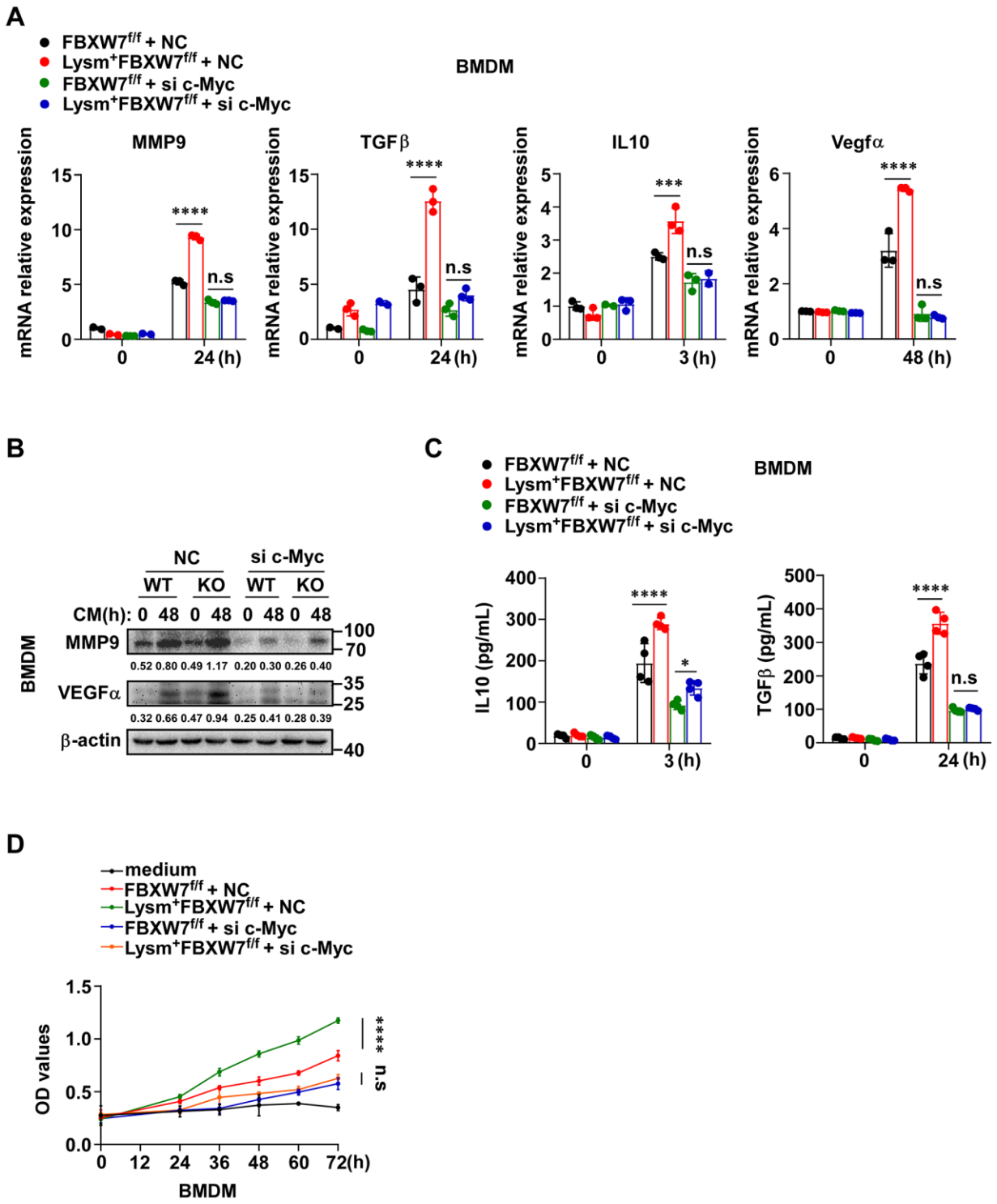

Supplementary Figure 6. The effect of FBXW7 on M2 macrophage expression of pro-tumoral factors is dependent on c-Myc. (**A**) qRT-PCR analysis of *MMP9*, *IL-10, TGFβ,* and *VEGFα* mRNA expression in BMDMs from FBXW7$^{f/f}$ and Lysm^{+}FBXW7$^{f/f}$ mice transfected with or without c-Myc siRNA and stimulated with conditioned medium. (**B**) Immunoblotting analysis of MMP9 and VEGFα expression in primary macrophages from FBXW7$^{f/f}$ and Lysm^{+}FBXW7$^{f/f}$ mice transfected with or without c-Myc siRNA and stimulated with conditioned medium. (**C**) The protein levels of IL10 and TGFβ in the supernatant of four groups were measured by ELISA kits. (**D**) LLCs were cultured in serum-free RPMI-1640, supernatant from IL-4-induced wild-type or FBXW7-knockout macrophages, supernatant from IL-4-induced wild-type or FBXW7-knockout macrophages transfected with c-Myc siRNA. The proliferation of LLCs in five groups was measured by the MTT assay. Data are shown as the mean ± SD and are representative of three independent experiments. **P* < 0.05; ****P* < 0.001; *****P* < 0.0001; n.s, no significance (two-way ANOVA (**A**, **C**, **D**)).

Supplementary Tables

Supplementary Table 1. A list of antibodies and reagents used in the study.

REAGENTS	SOURCE	Cat#
Antibodies		
β-Actin (Mouse mAb)	Protein Tech	60008-1-Ig
GAPDH (Mouse mAb)	Protein Tech	60004-1-Ig
FBXW7 (Rabbit mAb)	Abcam	12992
Phospho-c-Myc T58 (Rabbit mAb)	Abcam	185655
Ym1 (Rabbit mAb)	Abcam	93034
c-Myc (Rabbit mAb)	Cell Signaling Technology	9402
Phospho-ERK (Rabbit mAb)	Cell Signaling Technology	4370
ERK (Rabbit mAb)	Cell Signaling Technology	4695
Phospho-JNK (Rabbit mAb)	Cell Signaling Technology	9251
JNK (Rabbit mAb)	Cell Signaling Technology	9252
Phospho-AKT S473 (Rabbit mAb)	Cell Signaling Technology	4060
Phospho-AKT T308 (Rabbit mAb)	Cell Signaling Technology	13038
AKT (Rabbit mAb)	Cell Signaling Technology	9272
Phospho-STAT6 (Rabbit mAb)	Cell Signaling Technology	56554
Arginase-1 (Rabbit mAb)	Cell Signaling Technology	93668
K48-linkage specific polyubiquitin (Rabbit pAb)	Cell Signaling Technology	8081
STAT6 (Rabbit mAb)	Themo Fisher Scientific	MA5-15659
MMP9	Santa Cruz Biotechnology	sc-393859
VEGF	Santa Cruz Biotechnology	sc-7269
FC: CD45	biolegend	103116
FC: CD11c	biolegend	117310
FC: CD11b	biolegend	101206
FC: F4/80	biolegend	123131
FC: CD206	biolegend	141720
FC: CD3	biolegend	100236
FC: CD4	biolegend	100434
FC: B220	biolegend	103206
FC: Ly6G	biolegend	127639
FC: Ly6C	biolegend	128014
FC: CD163	biolegend	333613
FC; CD14	biolegend	367143
FC: CD11b	biolegend	301309
FC: MHCII	eBioscience	12-5321-82
FC: CD8	eBioscience	12-0081-82
Chemicals, Peptides, and Recombinant Proteins		
Recombinant Murine IL4	PeproTech	214-14

Cycloheximide (CHX)	Sigma Aldrich	C4859
MG132	Sigma Aldrich	M8699
Liberase TM	Roche	345474
DnaseI	Themo Fisher Scientific	EN0521
PMA	Sigma Chemical	P1585
Mouse IL10 uncoated ELISA	Invitrogen	88-7105
Human IL10 uncoated ELISA	Invitrogen	88-7106
Human/Mouse TGF beta1 uncoated ELISA	Invitrogen	88-8350
Experimental Models: Cell Lines		
Lewis lung carcinoma cells (LLCs)	The Cell Bank of The Chinese Academy of Science,Shanghai,China	TCM 7
A549	The Cell Bank of The Chinese Academy of Science,Shanghai,China	SCSP-503
THP-1	The Cell Bank of The Chinese Academy of Science,Shanghai,China	SCSP-567
Experimental Models: Organisms/Strains		
C57BL/6J mice	Model Animal Research Center of Nanjing University	N000013
$FBXW7^{f/f}$ C57BL/6J mice	the Jackson Laboratary	017563
Lysm-Cre C57BL/6J mice	Prof. Ximei Wu of Zhejiang University.	not available
Oligonucleotides		
siRNA targeting sequence:c-Myc#1 CCGTACAGCCCTATTTCAT	this paper	not available
siRNA targeting sequence:FBXW7 CCAGAGAAATTGCTTGCTT	this paper	not available
Software and Algorithms		
FlowJO	FlowJO	https://www.flowjo.com/
imageJ	imageJ	https://www.imagej.net/
Graphpad Prism 8	Graphpad software	http://www.graphpad.com

Supplementary Table 2. Primers for RT-PCR.

Gene (mouse)	Forward (5′-3′)	Reverse (5′-3′)
β-actin	AGTGTGACGTTGACATCCGT	GCAGCTCAGTAACAGTCCGC
Arginase-1	CTCCAAGCCAAAGTCCTTAGAG	AGGAGCTGTCATTAGGGACATC
Fizz1	CCAATCCAGCTAACTATCCCTCC	CCAGTCAACGAGTAAGCACAG
Ym1	CAGGTCTGGCAATTCTTCTGAA	GTCTTGCTCATGTGTGTAAGTGA
FBXW7	GTGATAGAGCCCCAGTTCCA	CCTCAGCCAAAATTCTCCAG
MMP9	CTGGACAGCCAGACACTAAAG	CTCGCGGCAAGTCTTCAGAG
IL-10	TGGCCCAGAAATCAAGGAGC	CAGCAGACTCAATACACACT
VEGFα	GGAGATCCTTCGAGGAGCACTT	GGCGATTTAGCAGCAGATATAAGAA
TGFβ	GAAGGCAGAGTTCAGGGTCTT	GGTTCCTGTCTTTGTGGTGAA
c-Myc	ATGCCCCTCAACGTGAACTTC	CGCAACATAGGATGGAGAGCA

Supplementary Table 3. Primers for RT-PCR.

Gene (human)	Forward (5′-3′)	Reverse (5′-3′)
β-actin	CTCCATCCTGGCCTCGCTGT	GCTGCTACCTCCACCGTTCC
Arginase-1	TGGACAGACTAGGAATTGGCA	CCAGTCCGTCAACATCAAAACT
CD163	GACGCATTTGGATGGATCATGT	CCCACCGTCCTTGGAATTTGA
IL10	TCAAGGCGCATGTGAACTCC	GATGTCAAACTCACTCATGGCT
TGFβ	CTAATGGTGGAAACCCACAACG	TATCGCCAGGAATTGTTGCTG